Architectural underpinnings of stochastic intergenerational homeostasis

Kunaal Joshi,* Charles S. Wright, Rudro R. Biswas,† and Srividya Iyer-Biswas‡
Department of Physics and Astronomy, Purdue University, West Lafayette, Indiana 47907, USA

(Received 26 November 2023; revised 27 March 2024; accepted 24 July 2024; published 27 August 2024)

Living systems are naturally complex and adaptive and offer unique insights into the strategies for achieving and sustaining stochastic homeostasis in different conditions. Here we focus on homeostasis in the context of stochastic growth and division of individual bacterial cells. We take advantage of high-precision long-term dynamical data that have recently been used to extract emergent simplicities and to articulate empirical intra- and intergenerational scaling laws governing these stochastic dynamics. From these data, we identify the core motif in the mechanistic coupling between division and growth, which naturally yields these precise rules, thus also bridging the intra- and intergenerational phenomenologies. By developing and utilizing techniques for solving a broad class of first-passage processes, we derive the exact analytic necessary and sufficient condition for sustaining stochastic intergenerational cell-size homeostasis within this framework. Furthermore, we provide predictions for the precision kinematics of cell-size homeostasis and the shape of the interdivision time distribution, which are compellingly borne out by the high-precision data. Taken together, these results provide insights into the functional architecture of control systems that yield robust yet flexible stochastic homeostasis.

DOI: 10.1103/PhysRevE.110.024405

I. INTRODUCTION

Robust architecture is a common feature of functional complex and adaptive systems. Strict constraints on protocols enable a plug-and-play modularity that confers flexibility to (or deconstrains) the overall systems design [1,2]. Recent high-precision experiments and analysis of extant data on different microorganisms have shown that stochastic intergenerational homeostasis of cell sizes is constrained by surprisingly universal and elegant emergent simplicities [3–6], despite the substantial differences in underlying molecular circuitry governing growth and division in system- and environment-specific ways. What robust architectures lead to the observed intra- and intergenerational emergent simplicities governing stochastic intergenerational homeostasis?

Between successive divisions, cell size increases stochastically while adhering to an intragenerational scaling law: The mean-rescaled cell-size distributions of cells at different times since the last division event undergo a scaling collapse [7,8] [see Fig. 1(c)]. The mean itself increases exponentially with time since the last division event [7,8]. Furthermore, intergenerational size dynamics is Markovian and a scaling law constrains the precision kinematics of stochastic intergenerational homeostasis: The distributions of the mean-rescaled size at birth in the next generation are independent of the sizes at birth in the current generation [3,4] [see Fig. 1(d)]. Intuitively, it is clear that these empirically observed scaling laws or emergent simplicities must reflect key aspects of the nature of the coupling of growth to division, but using the observed phenomenology to decipher the underlying mechanism has remained an open challenge. Here we provide the solution to this problem.

In addition to yielding the observed emergent simplicities, the minimal mechanistic model we propose here has inbuilt constraints that deconstrain, allowing for versatile implementations with different system-specific details for different microorganisms (or even growth conditions) while robustly ensuring that homeostasis will result in each instantiation, despite the inherent stochasticity in the growth and division processes. From the point of view of evolvability, conserved core functional architectures serve to constrain variation that would break the core mechanism. On the balance, they confer flexibility and robustness to processes that leave the core intact [1,2].

We start with the minimal model that reproduces the observed universal statistics of cell-size growth, namely, the stochastic Hinshelwood cycle (SHC) model of stochastic exponential growth [7–10]. Let X represent the effective SHC variable undergoing stochastic exponential growth according to [7,10]

$$X \xrightarrow{k_X} X + X. \tag{1}$$

It relates to the cell size a via

$$a(t) = X(t)/\lambda, \tag{2}$$

where λ is a scaling factor relating the discrete copy numbers of X to the cell size a. The previously noted intragenerational scaling law is consistent with this model, since in balanced growth conditions it naturally yields

$$P(X,t) = e^{-k_X t} P_0(X e^{-k_X t}), \tag{3}$$

*Contact author: joshi84@purdue.edu
†Contact author: rrbiswas@purdue.edu
‡Contact author: iyerbiswas@purdue.edu

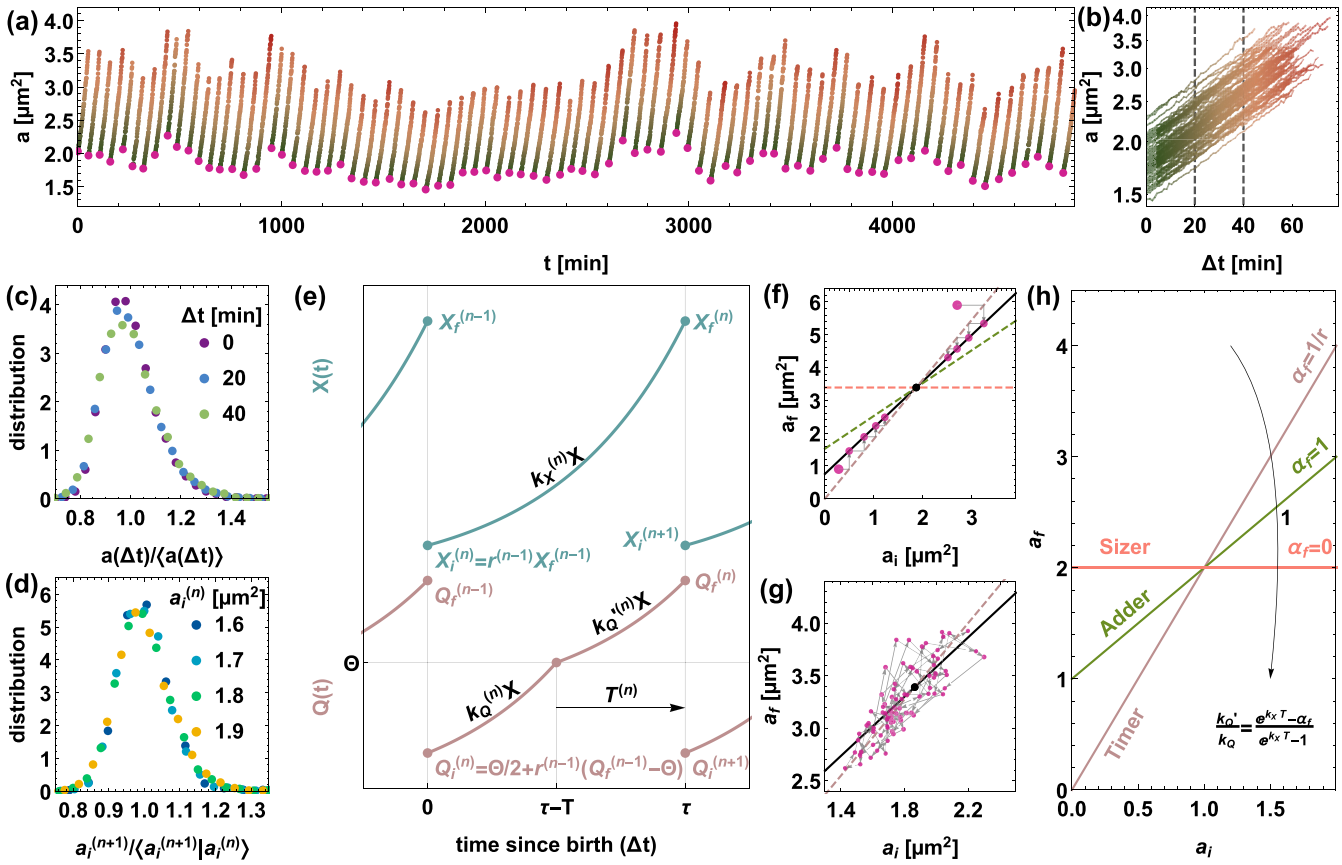

FIG. 1. Empirically observed emergent simplicities motivate the mechanistic model for stochastic intergenerational homeostasis. (a) Stochastic intergenerational homeostasis of cell sizes at birth (highlighted magenta circles) as seen in high-precision data recording an individual cell's stochastic growth and division dynamics over multiple generations. (b) Cell sizes in (a) replotted on a log-linear scale versus time since the last division event Δt; cell sizes undergo stochastic exponential growth between divisions. (c) Distributions of cell sizes at different times since birth [marked by the gray dashed lines in (b)] plotted after rescaling by their respective mean values. These mean-rescaled distributions undergo a scaling collapse, an intragenerational scaling law consistent with the stochastic Hinshelwood cycle model of stochastic exponential growth. (d) Conditional distributions of the next generation's initial size given the current generation's initial size plotted for the specified current initial sizes, after rescaling by their corresponding mean values. These mean-rescaled distributions undergo a scaling collapse revealing an intergenerational scaling law, which in turn specifies the precision kinematics of stochastic cell-size homeostasis. (e) The proposed mechanistic model bridges the intra- and intergenerational cell growth and division dynamics. Here X is the effective Hinshelwood cycle variable corresponding to cell size, while Q represents the thresholding species; $X_i^{(n)}$ and $Q_i^{(n)}$ are the copy numbers of X and Q at birth in the nth generation and $X_f^{(n)}$ and $Q_f^{(n)}$ are the copy numbers at division. Throughout the cell cycle, X is produced at rate $k_X^{(n)}X$. Initially, Q is produced at rate $k_Q^{(n)}X$, until it crosses the threshold at Θ, after which time its production rate is reset to $k_Q'^{(n)}X$. After crossing the threshold, cell division occurs after time T. Upon division, the next generation's X_i and Q_i values are related to the current generation's X_f and Q_f values through the division rules given by Eq. (10). The proposed stochastic model naturally yields the observed phenomenologies in (a)–(d) and (g). (f) Heuristic argument for intergenerational homeostasis in extant models based on the deterministic sizer-timer-adder paradigms. Within this scheme, the intergenerational final size a_f vs the initial size a_i dynamic is thought to occur as shown: Starting from an initial generation characterized by the coordinates of the large magenta circle, the cell deterministically adjusts its size to exponentially relax to the target cell size set by the black dot at the intersection between lines corresponding to the growth and division rules. (g) In contrast to the heuristics suggested by the extant sizer-timer-adder paradigms [shown in (f)], the experimentally observed high-precision intergenerational a_f vs a_i trajectories [here taken from the cell shown in (a)] are dramatically and quantitatively different, thus motivating the necessity for a completely revised framework. (h) In the appropriate ranges of parameter values, the fully stochastic mechanistic model we propose here can recapitulate specific mean behaviors displayed by the sizer-timer-adder paradigm. For the mean final size given the initial size in the quasideterministic limit, the slope α_f is controlled by the relative rate of production of Q after crossing the threshold k_Q'/k_Q. In the deterministic limit, slopes $\alpha_f = 0, 1, 1/r$ (with k_Q' greater than, equal to, and less than k_Q, respectively) correspond to sizer, adder, and timer models, where r is the deterministic division ratio.

where P_0 is an initial condition-dependent distribution [7–10]. Since the mean grows as $e^{k_X t}$ with time, when this distribution at any given time is rescaled by its mean value, a time-invariant distribution results.

Additionally, since the cell-size-at-birth distribution must satisfy the intergenerational scaling governing stochastic intergenerational homeostasis, so must the copy numbers of X at birth, i.e., immediately following a division

event [3,4],

$$P_1(X^{(n+1)}|X^{(n)}) = \frac{1}{\mu(X^{(n)})}\Pi\left(\frac{X^{(n+1)}}{\mu(X^{(n)})}\right), \tag{4}$$

where P_1 is the conditional distribution of $X^{(n+1)}$ (the next generation's initial copy numbers, i.e., copy numbers at birth) given $X^{(n)}$ (the current generation's initial copy numbers), μ is the next generation's mean initial copy number as a function of the current generation's initial copy number, and Π is the invariant distribution that results after mean rescaling P_1. This emergent simplicity, as we have derived in [4], specifies the precision kinematics of initial copy numbers over successive generations through the exact stochastic map

$$X^{(n+1)} = s^{(n)}\mu(X^{(n)}), \tag{5}$$

where the $s_i^{(n)}$ are random numbers drawn from the distribution Π (with unit mean); the superscript serves to record the generation as n. In sum, in the formulation we have presented here, the specific challenge is to bridge intra- and intergenerational phenomenologies by identifying the correct mechanistic coupling between growth and division that naturally yields the intergenerational scaling law (4).

II. RESULTS

A. Mechanistic underpinnings of stochastic intergenerational homeostasis

A minimal model consistent with empirical observations can be articulated as follows (see Fig. 1 for a graphical summary). As outlined in Eqs. (1) and (2), the copy numbers of X serve as a proxy for cell size a and undergo stochastic exponential growth. The mechanism of size control is implemented by an auxiliary growth reporter Q, whose numbers increase stochastically with a propensity proportional to the copy numbers of X present:

$$X \xrightarrow{k_Q} Q + X. \tag{6}$$

When Q reaches a threshold value of Θ, the decision to commit to division is taken and a stochastic process commences, culminating in cell division after a random delay time T. In this post-threshold period (of duration T), the X-Q dynamics continues to proceed as in Eqs. (1) and (6); however, the propensity of production of Q may differ and is thus denoted by k'_Q. Here we consider the quantities T, k_X, k_Q, and k'_Q to be constant through a given generation, but treat them as intergenerational stochastic variables that vary from generation to generation (and cell to cell when population-level distributions are constructed). Finally, cell division occurs with the copy numbers reset according to Eq. (10) and governed by the division ratio r, a random variable we assume to be independent of cell size. For symmetrically dividing cells, the mean division ratio is $1/2$.

B. Intragenerational statistics: Exact analytic solution

While several techniques are known for solving for stochasticity arising due to copy number fluctuations in different models [11–17], an exact analytic solution to the problem of coupled stochastic evolution of X and Q, as encoded in Eqs. (1) and (6), respectively, is not readily derived via traditional approaches. Instead, we solve this seemingly intractable problem (below) through a stochastic rescaling of time. Our method relies on the fact that while X influences the growth of Q through the rate $k_Q \times X$, Q does not influence the stochastic growth dynamics of X. Our mathematical technique is broadly applicable to scenarios where the growth rates for both Q and X are arbitrary functions of X.

We define a new rescaled time variable t_r whose rate of change with the laboratory time variable t is just the growth rate of Q:

$$\frac{dt_r}{dt} = k_Q X(t). \tag{7}$$

When the laboratory time t is replaced by t_r, from Eqs. (1) and (6) we see that the dynamics of Q becomes formally X independent, while the growth rate of X becomes the ratio of its laboratory growth propensity to that of Q, also formally independent of X. Thus, when the time variable is t_r, the dynamics become that of two uncoupled growth reactions, schematically represented as

$$\phi \xrightarrow{k_r} X, \quad \phi \xrightarrow{1} Q, \tag{8}$$

with $k_r = k_X/k_Q$. In terms of this rescaled time, the coevolution of X and Q can be obtained analytically, even though characterizing their coevolution in laboratory time is difficult. Specifically, using standard techniques of stochastic processes [11,12], we have calculated analytically that the distribution of $X = X_\Theta$ when Q reaches the threshold value of Θ, when starting from initial values (X_i, Q_i), is a Pascal distribution

$$P_{X_\Theta}(X_\Theta) = \frac{(\Delta X + \Delta Q - 1)!}{\Delta X!(\Delta Q - 1)!}\frac{(k_r)^{\Delta X}}{(1 + k_r)^{\Delta X + \Delta Q}}, \tag{9}$$

where $\Delta X = X_\Theta - X_i \geqslant 0$ and $\Delta Q = \Theta - Q_i \geqslant 1$ (see Appendix 1).

Quasideterministic limit

We now consider an interesting limit of this process, which is useful for comparison with experimental data. From the above distribution, the ratio of the standard deviation to the mean for ΔX is $\sqrt{(1 + k_r)/k_r \Delta Q}$. Since $k_r \gg 1$ is the physical regime of interest where the numbers of Q are very small compared to the numbers of X and since in steady state $\Delta Q \sim \Theta$ up to a fractional factor $1/2$, we find that for large Θ the standard deviation becomes negligible compared to the mean [their ratio becomes approximately $\sqrt{(1 + 1/k_r)/\Theta}$]. In this regime, the distribution of $\Delta X_\Theta \simeq k_r \Delta Q$ becomes an almost deterministic function of Q_i. Furthermore, if k'_Q/k_Q is negligible and division noise is limited, Q_i is just a constant times Θ. In summary, for $\Theta \gg 1 + 1/k_r$, ΔX_Θ becomes quasideterministic; furthermore, when $k'_Q \ll k_Q$, its value is a function only of Θ and k_r and thus independent of X_i (see Appendix 4). In other words, in this limit, a constant amount is added to X_i during the time taken for Q to reach the threshold.

As outlined previously, once the thresholding of X_Θ occurs, a division process commences that lasts time T, following which the cell divides with division ratio r. (Note that both

T and r are random variables whose values change from generation to generation.) During this process, X and Q continue to grow following Eqs. (1) and (6), with $k_Q \to k'_Q$. We have analytically solved the corresponding master equation and found the joint moment-generating function for the final predivision copy numbers (X_f, Q_f), starting from the respective values at the threshold (X_Θ, Θ) (Appendix 2). Combining the analytic results [Eq. (9)] for the statistics of X_Θ, we have analytically calculated the statistics of (X_f, Q_f), given initial values (X_i, Q_i) (see Appendix 2). These statistics completely specify the intragenerational stochastic evolution of cell size in our framework and are used in the following sections.

C. Intergenerational statistics: Homeostasis condition

We now proceed to determine the intergenerational evolution of (X, Q), and hence the cell size. This is provided by the division rule that converts the final predivision values in a given generation, (X_f, Q_f), to the initial values (X_i, Q_i) in the next generation. Using the notation $A^{(n)}$ to represent the value of a random quantity A measured in generation n, we propose the following division rules that incorporate the cell-size division ratio r:

$$X_i^{(n+1)} = r^{(n)} X_f^{(n)}, \tag{10a}$$

$$Q_i^{(n+1)} = \frac{\Theta}{2} + r^{(n)}\big(Q_f^{(n)} - \Theta\big). \tag{10b}$$

For asymmetrically dividing cells, we underscore the subtle point that a portion of Q, equal to the threshold amount Θ, is split equally during division among the daughter cells and not at the division ratio r. Biochemically, such behavior may naturally arise, for instance, if an amount Θ of Q accumulates around the cell division plane to initiate division. This assumption is not necessary for achieving cell-size homeostasis but is consistent with the experimentally observed simplicities discussed in the following sections. The implications of alternate division rules are explored in Appendix 5. In a later section, we discuss possible biological implementations and implications in greater detail.

We can now consider the question of the homeostatic stability of the intergenerational evolution of X and consequently cell size. Addressing this problem requires consideration of the intergenerational coevolution of both X and Q. However, since the absolute amount of Q is constrained at the thresholding point in every generation, Q is trivially in homeostasis. We can thus simply consider the intergenerational evolution of the value of X at a fixed point in the cell cycle. Specifically, we choose to follow the intragenerational evolution of X_Θ, since at that thresholded event the value of Q must be Θ and thus its coevolution is trivial. For a given generational history of values of T, r, k_X, k_Q, and k'_Q, we find the following intergenerational evolution of the reaction noise-averaged moments of X_Θ, $\mu_m = \langle (X_\Theta)^m \rangle$ for $m \geqslant 1$ (see Appendix 2 for details; we define $\mu_0 = 1$):

$$\mu_m^{(n+1)} = (A^{(n)})^m \mu_m^{(n)} + \sum_{m'=0}^{m-1} \tilde{A}_{mm'}^{(n)} \mu_{m'}^{(n)}, \tag{11a}$$

where

$$A^{(n)} = r^{(n)} \left[e^{k_X^{(n)} T^{(n)}} - \frac{k_Q'^{(n)} k_X^{(n+1)}}{k_Q^{(n+1)} k_X^{(n)}} \big(e^{k_X^{(n)} T^{(n)}} - 1 \big) \right], \tag{11b}$$

and $\tilde{A}_{mm'}^{(n)}$ are bounded quantities whose exact forms are unimportant for the homeostasis of X_Θ and thus cell size. Under intergenerational evolution in accordance with the above equations, attainment of stochastic homeostasis is assured, provided, as $n \to \infty$, all moments $\mu_m^{(n)}$ (i) become independent of the initial value $\mu_m^{(0)}$ and (ii) remain finite. Assuming that the $A^{(n)}$ are uncorrelated for different n, being independent draws of a random variable A, we have derived (see Appendix 3) the necessary and sufficient conditions for strict cell-size homeostasis, which we define as the existence of an initial-condition-independent homeostatic distribution, as the set of bounds on the moments of A,

$$\left| \overline{A^k} \right| < 1, \quad k = 1, 2, \ldots, \tag{12}$$

where the overline denotes an average over generations. As shown previously in [4], this sequence of conditions is equivalent to a simple bound on A: $|A|_{\max} \leqslant 1$. (The inequality is strict only if A is deterministic. If the inequality is violated for $k = k_0$, all moments μ_k with $k \geqslant k_0$ are unstable, i.e., do not reach homeostatic initial-condition-independent finite steady-state values [4].) These general conditions are reminiscent of conditions derived in the phenomenological theory in [4], corresponding to emergent simplicities in cell-size homeostasis observed in experiments [3]. We note that the existence of an initial-condition-independent homeostatic distribution necessitates that all moments exist. When a subset of these conditions is violated, the divergent higher-order moments would lead to a fat-tailed distribution resulting in occurrences of abnormally large cells albeit with low probability, which in principle could be biologically possible.

1. Quasideterministic limit

The quasideterministic limit applies when the copy numbers of X and Q are large enough that the reactions in Eqs. (1) and (6) proceed deterministically. This applies when $X_i, Q_i \gg 1$ (consistent with the condition $\Theta \gg 1 + 1/k_r$ considered earlier). In this limit, intragenerational dynamics proceed deterministically, and the primary source of noise in the system is due to the intergenerational variation of reaction rates k_X, k_Q, and k'_Q and the duration between threshold crossing and division, T. By Eq. (1) our model cell undergoes quasideterministic exponential growth, in agreement with high-precision experimental observations of exponential growth in bacterial cells under constant nutrient-rich growth conditions [8]. Meanwhile, intergenerational evolution of cell size is encapsulated in the relation between initial sizes of successive

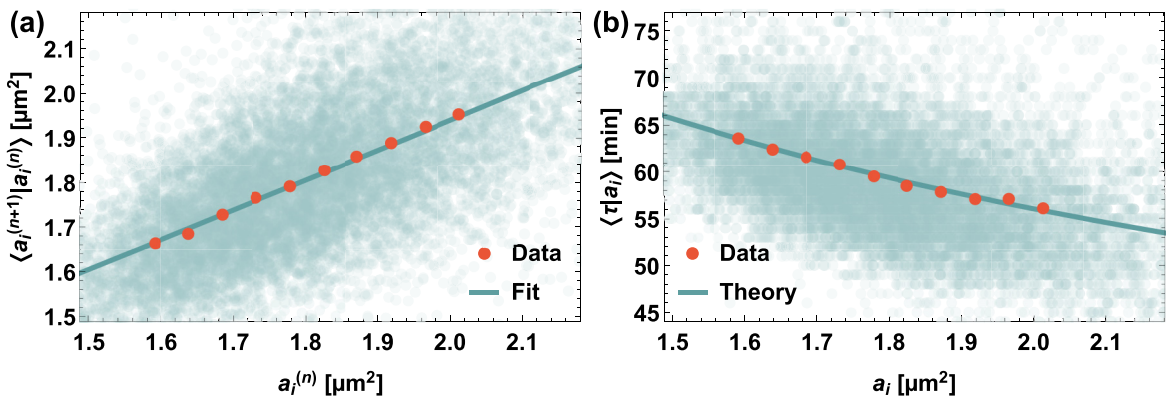

FIG. 2. Parameter estimation, with theoretical predictions validated by experimental data. (a) Experimentally measured mean (red circles, with error bars) of the next generation's initial area plotted as a function of the current generation's initial area. The only fitting parameter in the model, $k_r\Theta/\lambda$, is estimated as twice the intercept over the slope of the linear fit to the mean [see Eq. (17)]. The light teal scatter plot in the background shows the next generation's initial area versus the current generation's initial area for different cell cycles in the data. (b) Experimentally measured mean (red circles, with error bars) of the division time plotted as a function of the initial area. The teal curve is the analytic model prediction given by Eq. (23). Note that the error bars are small compared to the marker size and hence are not visible.

generations (see Appendix 4):

$$a_i^{(n+1)} = r^{(n)} e^{k_X^{(n)} T^{(n)}} \left(\frac{k_X^{(n)}\Theta}{2k_Q^{(n)}\lambda} + \left[1 - \frac{k_Q'^{(n-1)} k_X^{(n)}}{k_Q^{(n)} k_X^{(n-1)}} \left(1 - e^{-k_X^{(n-1)} T^{(n-1)}}\right) \right] a_i^{(n)} \right). \tag{13}$$

2. *Recapitulating known results for mean behaviors*

The mean of the final size a_f given the initial size a_i is found to vary linearly with the initial size for nearly all bacterial species studied [18],

$$\langle a_f | a_i \rangle = \alpha_f a_i + \beta_f, \tag{14}$$

for constants α_f and β_f that are species and condition dependent. Traditional deterministic homeostasis models consider the final size a_f of a cell with initial size a_i to be equal to $\langle a_f | a_i \rangle$ and hence to follow the deterministic map $a_i^{(n+1)} = \alpha a_i^{(n)} + \beta \equiv \mu(a_i^{(n)})$, where α and β are equal to $\langle r \rangle \alpha_f$ and $\langle r \rangle \beta_f$, respectively; $\langle r \rangle$ is the average division ratio; and μ is the mean function in Eq. (5). For such a deterministic map, a_n converges to a finite value independent of a_0 as $n \to \infty$ if and only if $|\alpha| < 1$ [19,20]. This formulation has been used for the adder ($\alpha = \langle r \rangle$), timer ($\alpha = 1$), and sizer ($\alpha = 0$) models [21–26] [Figs. 1(f) and 1(h)]. Although these models adequately describe mean trends, they fundamentally fail to capture the observed stochastic dynamics, governed by the stochastic map given by Eq. (5), which results from the intergenerational scaling law (4). That the mythical "average" cell fails to capture the stochastic behaviors of the individual bacterial cell is increasingly well appreciated in different contexts [3,4,6,27–32]. Starting with Eq. (13), taking an intergenerational average over the stochastic variables k_X, k_Q, k_Q', and T results in the prediction that the conditional mean of the next generation's initial size given the current generation's initial size varies linearly with the current generation's initial size, consistent with observations above. Moreover, the ratio k_Q'/k_Q can be used to tune the slope α [Fig. 1(h)]. Slopes between the pure adder and pure timer require $k_Q' < k_Q$, the slope for the pure adder requires $k_Q' = k_Q$ (or trivially when $T = 0$ and the model becomes k_Q' independent), and slopes between the pure sizer and pure adder can be obtained when $k_Q' > k_Q$.

D. Comparison with data: Emergent simplicities and parameter extraction

Incorporating into Eq. (5) the observed linear dependence of the mean $\mu(a) = \alpha a + \beta$, which is also reproduced by our model (see the preceding section), the significant emergent simplicity governing intergenerational cell-size evolution is [3,4]

$$a_i^{(n+1)} = s^{(n)} \left(\alpha a_i^{(n)} + \beta \right), \tag{15}$$

where $a_i^{(n)}$ is the initial newborn size in the nth generation, the numbers $\{s^{(n)}\}$ are independent random instantiations of a random variable s with unit mean and a growth condition-dependent probability distribution, and (α, β) are the growth condition-dependent constants determining the mean μ [Fig. 2(a)]. This simplicity straightforwardly emerges from our model in the quasideterministic limit when $k_Q' = 0$ and $\Theta \gg 1 + 1/k_r$ (also $X \gg Q$). Here we can set k_Q' to zero since the experimental data showing this emergent simplicity are obtained from *Caulobacter crescentus* cells. For these cells, the slope of the conditional mean of the next generation's initial size given the current generation's initial size lies between those of the pure adder and pure timer; hence $k_Q' = 0$ satisfies the required constraint $k_Q' < k_Q$. Since $k_Q' = 0$, at the end of each cell generation $Q = Q_f = \Theta$. Using Eq. (10), in steady state the initial amount of Q is always $Q_i = \Theta/2$. As observed previously, when $\Theta \gg 1 + 1/k_r$, X_Θ is quasideterministic and results from adding a

constant amount to X_i: $X_\Theta \simeq X_i + k_r \Delta Q = X_i + k_r\Theta/2$. Due to quasideterministic exponential growth through the period T of the subsequent division process, X increases further to $X_f = e^{k_X T} X_\Theta = e^{k_X T}(X_i + k_r\Theta/2)$. Converting from X to cell size a using Eq. (1) and applying Eq. (10), our model yields

$$a_i^{(n+1)} = r^{(n)} e^{k_X^{(n)} T^{(n)}} \left(a_i^{(n)} + k_r\Theta/2\lambda\right). \tag{16}$$

Taking into account the intergenerational stochasticity of r, T, and k_X, this stochastic map is equivalent to the emergent scaling law for intergenerational cell-size control [Eq. (15)], obtained from experimental data. We can identify the observed constants in this law with the parameters of our model:

$$\alpha = \overline{re^{k_X T}}, \quad \lambda\beta = \overline{re^{k_X T}} k_r\Theta/2,$$
$$s^{(n)} = \frac{r^{(n)} e^{k_X^{(n)} T^{(n)}}}{\overline{re^{k_X T}}}. \tag{17}$$

As before, the overline denotes an intergenerational average and $k_r = k_X/k_Q$ (assumed constant). Conversely, we can estimate the following model parameters and distributions from intergenerational growth and division data [see Fig. 2(a)]:

$$\frac{k_r\Theta}{\lambda} = \frac{2\beta}{\alpha}, \quad T^{(n)} = \frac{1}{k_X^{(n)}} \ln\left(\frac{a_f^{(n)}}{a_i^{(n)} + \beta/\alpha}\right). \tag{18}$$

Note that the first relation of (18) applies not only in the quasideterministic limit, but also in the nonapproximate case (see Appendix 6). We have extracted the values of α and β from experimental data in Fig. 2(a) and shown a match in the predictions consistent with Eq. (14) in Fig. 2(b).

In conclusion, k_X is the experimentally measured cell-size growth rate, $k_Q' = 0$, and k_Q is proportional to k_X with a constant of proportionality $k_r = k_X/k_Q$. The constant $k_r\Theta/\lambda$ is the only fitted parameter in our model, obtained through Eq. (18) and the extracted values of α and β from the data fit in Fig. 2(a). Once this is obtained, T can be measured from individual cell cycles through Eq. (18), and the joint distributions of r, T, and k_X compiled. The data do not yield values of Θ, k_r (or equivalently $k_Q = k_X/k_r$), or λ individually; however, these are constrained by our assumption of intragenerational noise-free growth ($\Theta \gg 1 + 1/k_r$) and allow for a range of combinations that provide data-theory matches. Combining with Eq. (18), we require for self-consistency

$$\Theta \gg \frac{1}{1 - \frac{\alpha}{2\beta\lambda}}, \quad k_r \ll \frac{2\beta\lambda}{\alpha} - 1. \tag{19}$$

For large values of $\beta\lambda$, which correspond to large numbers of X in the cell, the first condition becomes simply $\Theta \gg 1$, i.e., the cell contains a large number of Q, even though these may be far fewer in number than X.

E. Exact solution and robust predictions

With $k_Q' = 0$, the exact solution for the distribution of copy numbers of X at division, X_f, given initial copy numbers X_i is (see Appendix 6)

$$P_f(X_f|X_i) = \sum_{x=X_i}^{X_f} \binom{X_f - 1}{x - 1} (1 - e^{-k_X T})^{X_f - x} e^{-x k_X T} \times \binom{x - X_i + \Theta/2 - 1}{\Theta/2 - 1} \left[\frac{k_r}{1 + k_r}\right]^{x - X_i} \left[\frac{1}{1 + k_r}\right]^{\Theta/2}. \tag{20}$$

The above distribution is the predicted distribution for a single cell cycle with given k_X and T values. The overall distribution can be obtained by taking the intergenerational average with respect to the (observed) joint distribution of k_X and T. From this analytic result we can find the distribution of the next generation's initial size by multiplying the current generation's final size (equal to X_f/λ) by the division ratio r and then taking the intergenerational average with respect to the observed joint distribution of k_X, T, and r.

Our analytic results for the distribution of the next generation's initial cell size, conditioned on the current generation's initial cell size, are compared with experimental data in Fig. 3. There is superb agreement between experiment and theory. The exact size distributions predicted by our model also undergo the experimentally observed intergenerational scaling collapse. Our mechanistic model can thus generate the experimentally observed multigenerational size data on single cell growth and division with quantitative accuracy. Furthermore, we reiterate that our model predictions robustly match these dynamics irrespective of the exact choice of model parameters, provided the chosen parameters satisfy the constraints given by Eqs. (18) and (19) (see Figs. 7–9).

1. Condition for stochastic intergenerational size homeostasis

Given the scaling rule (15) for the intergenerational evolution of cell size, the conditions governing strict cell-size homeostasis have been shown to be [4]

$$\overline{(\alpha s)^k} < 1, \quad k = 1, 2, \ldots. \tag{21}$$

Since obtaining Eq. (15) from our model necessitates setting $k_Q' \to 0$, using this condition in Eqs. (17) and (11a), we find that $\alpha s = A$. Thus the experimentally relevant cell-size homeostasis conditions (21) are identical to the more general conditions corresponding to homeostasis in our model [Eq. (12)] in the limit where our model is consistent with experimental data.

In [3] we show that the stochastic map (15) accurately predicts the observed dynamics of initial cell sizes over successive generations, leading to cell-size homeostasis. However, we have shown above that this stochastic map is also obtained in the quasideterministic limit of our mechanistic model, which should enable us to generate the full intergenerational evolution of cell sizes. In Fig. 4 we show this evolution starting from different initial sizes. Our model accurately predicts the observed distributions of cell sizes over successive generations leading to cell-size homeostasis.

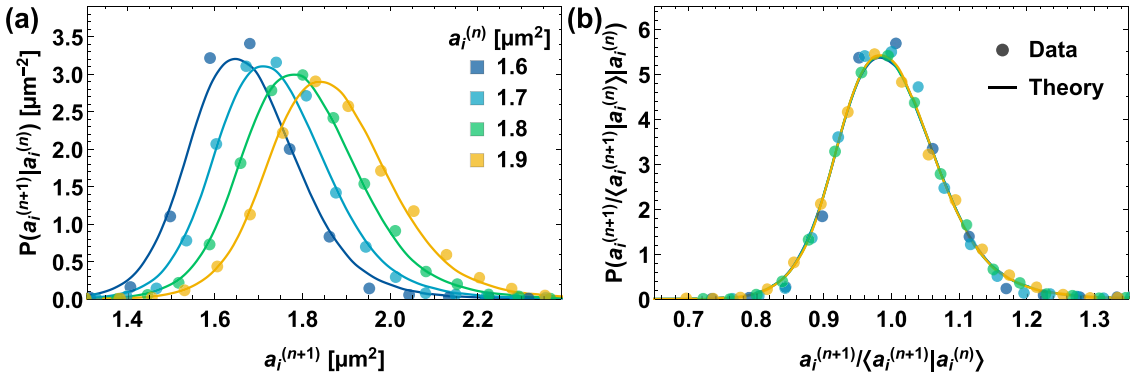

FIG. 3. Intergenerational scaling law: experimental data and predictions from the mechanistic model. (a) Conditional distributions of the next generation's initial areas $a_i^{(n+1)}$ given the current generation's initial areas $a_i^{(n)}$ plotted for four different current initial areas (marked by different colors). The solid lines are the results of exact model simulations, while the points represent experimental data. (b) Both experimentally measured and theoretically calculated distributions in (a) overlap when rescaled by their respective mean values.

2. Division time distribution

Using the quasideterministic limit (18), the cell division time $\tau = \ln(a_f/a_i)/k_X$ becomes

$$\tau = T + \frac{1}{k_X}\ln\left(1 + \frac{\beta/\alpha}{a_i}\right). \tag{22}$$

Here τ, T, k_X, and a_i are from the same generation. From this we predict that when a_i is fixed, the mean division time is just

$$\langle\tau\rangle_{a_i} = \langle T\rangle + \left\langle\frac{1}{k_X}\right\rangle\ln\left(1 + \frac{\beta/\alpha}{a_i}\right), \tag{23}$$

where $\langle\cdot\rangle$ and $\langle\cdot\rangle_{a_i}$ denote averaging over all generations or generations restricted by initial-size value a_i, respectively. This predicted functional form is compared against experimental values of $\langle\tau\rangle_{a_i}$ in Fig. 2(b), showing excellent agreement.

Furthermore, using the experimentally measured joint distribution of k_X and T, $P_{k_X,T}(k_X, T)$, and the model-predicted steady-state initial-size distribution $P_{a_i}(a_i)$ obtained through numerical methods described above and shown as the theoretical initial condition-independent homeostatic distribution in Fig. 4(f), our framework yields both the detailed conditional division time distribution for a given initial size $P_\tau(\tau|a_i)$ and, by averaging over a_i using the homeostatic size distribution, the full steady-state division time distribution $P_{\tau,\mathrm{SS}}(\tau)$:

$$P_\tau(\tau|a_i) = \int dk_X P_{k_X,T}\left[k_X, \tau - \frac{1}{k_X}\ln\left(1 + \frac{\beta/\alpha}{a_i}\right)\right], \tag{24a}$$

$$P_{\tau,\mathrm{SS}}(\tau) = \int da_i P_\tau(\tau|a_i)P_{a_i}(a_i). \tag{24b}$$

In Fig. 5 we show both conditional and full steady-state division time distributions obtained through the exact Gillespie simulations of our mechanistic model. While the chosen model parameters (the same as used to derive analytic results in previous sections) satisfy the conditions for the quasideterministic limit, the simulations are exact and do not assume quasideterministic simplifications. Once again, predictions match compellingly with the corresponding experimental data (see Fig. 5).

3. Biological identities of X and Q

Bacterial cell division involves assembly of the division machinery (divisome) followed by cell wall constriction and ultimate cleavage [33]. One of the earliest models of cell division hypothesized a diffusible factor that initiates division upon accumulation to a critical level [34]; this factor was later suggested to be the tubulin homolog FtsZ, whose assembly dynamics is driven by cell growth rate [35]. FtsZ is a critical player in recruiting and regulating members of the divisome, including cell wall remodelers responsible for synthesis and placement of peptidoglycan (PG) at the site of constriction [36,37], via formation of the Z ring at the future division site [38]. FtsZ exists in two conformations, found in monomer form or in (proto)filaments, respectively [39], which exhibit cooperative assembly such that additional monomers above a critical concentration increase only the polymer concentration [40,41]. The structure of the Z ring is dynamic, with FtsZ exhibiting treadmilling (continuous polymerization and depolymerization at opposite ends of a filament) [42], typically at a rate of 30–40 nm/s, although the details are species specific [43]. FtsZ treadmilling has been hypothesized to distribute PG synthesis and coordinate construction of the nascent endcaps by moving proteins around the division site [33]; indeed, its dynamics has been confirmed to correlate with populations of moving PG enzyme complexes in *Escherichia coli* [44] and *Bacillus subtilis* [45], and in *C. crescentus* the FtsZ-binding partner FzlA links it to PG synthesis [46]. In *B. subtilis*, FtsZ treadmilling is essential to mediate condensation of diffuse FtsZ filaments into a dense Z ring and to initiate constriction [47]. Numerous lines of evidence suggest that FtsZ's intrinsic capacity for polymerization provides the capability for Z-ring assembly, whereas its intrinsic GTPase activity is responsible for treadmilling dynamics, independent of other proteins or the cell cycle [48].

We propose that Q in our model may be identified with FtsZ, with the threshold value of Θ being the amount required for constriction initiation and the time delay T the interval between constriction initiation and cell division. To support this proposition, we consider the supporting evidence first for *E. coli* and then for *C. crescentus*. In *E. coli*, FtsZ is produced

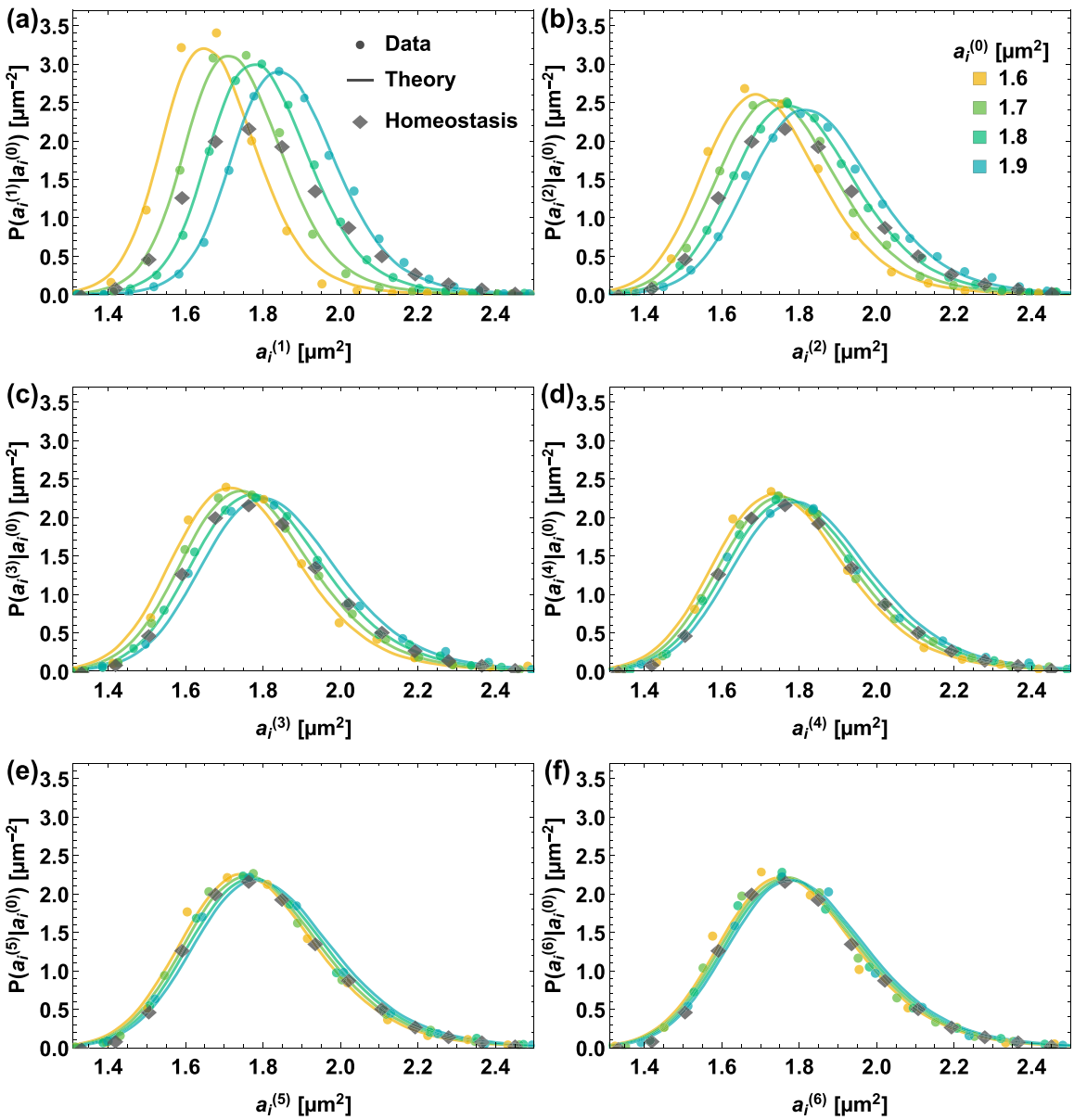

FIG. 4. Precision kinematics of stochastic intergenerational homeostasis: experimental data and predictions from the mechanistic model. Conditional distributions of initial sizes after n generations $a_i^{(n)}$, conditioned on the starting generation's initial size $a_i^{(0)}$, plotted for (a) $n = 1$, (b) $n = 2$, (c) $n = 3$, (d) $n = 4$, (e) $n = 5$, and (f) $n = 6$. The four different starting initial areas $a_i^{(0)}$ correspond to different colors. The solid lines are theoretical predictions based on exact simulations of the mechanistic model, while the points are experimentally measured data. The diamonds denote the experimentally measured populationwide homeostatic initial area distribution. All conditional distributions converge to this distribution as n increases, irrespective of the starting initial area.

at a constant rate per unit volume, with cells accumulating FtsZ molecules constitutively to maintain a constant concentration of FtsZ [49]. Constriction initiation coincides with maximal Z-ring intensity [50], followed by rapid proteolytic degradation at the end of division [51]. These observations are consistent with the picture in which FtsZ is produced at a rate proportionate to cell volume (represented by the effective stochastic Hinshelwood cycle variable X), with k_Q depending on condition-specific factors [38]. Furthermore, a recent large-scale phenotyping study of *E. coli* across a range of nutrient conditions and perturbations observed that FtsZ is required for constriction initiation, which occurs after a constant mean cell length has been added, and that division follows constriction initiation with a constant time delay [52], consistent with our model.

In the asymmetrically dividing *C. crescentus*, the picture is more complicated, as FtsZ levels are regulated in a cell-cycle-dependent manner [53], with synthesis beginning slightly before swarmer cells differentiate into stalked cells and concentration reaching a maximum at the beginning of cell division, followed by a precipitous drop [54]. Transcription of *ftsZ* in swarmer and predivisional cells is repressed by the master cell-cycle regulator CtrA [55], with transcription rates of *ftsZ* in stalked cells modulated by additional factors

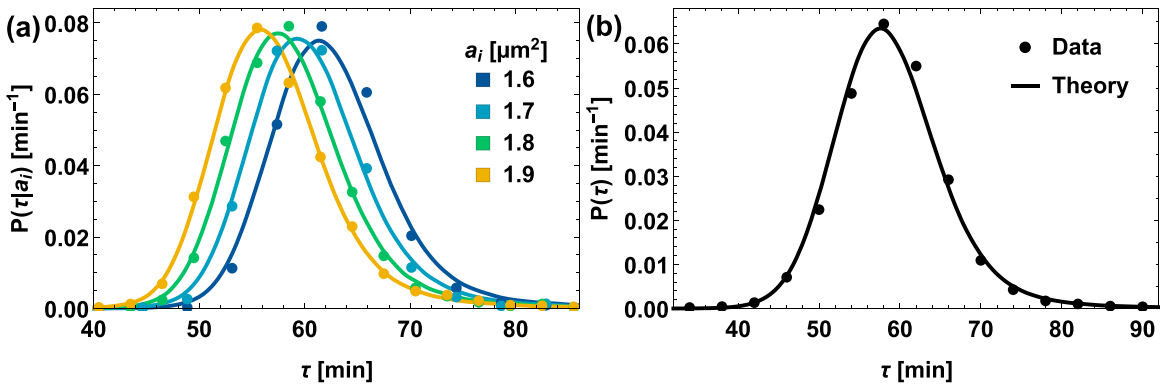

FIG. 5. Shape of the interdivision time distribution, with experimental data and predictions from the mechanistic model. (a) Division time distributions disambiguated by initial area plotted for different initial areas (distinguished by different colors). The solid lines are the theoretical predictions from the mechanistic model, while the points are experimentally measured data. (b) Full division time distribution.

such as nitrogen and carbon availability [56]. Although FtsZ is stable in the daughter stalked cell following cell division, it is cleared from the daughter swarmer cell [55,57] via a regulated proteolysis that appears intrinsic to the asymmetric cell division of *C. crescentus* [58]. Despite the complexity of this picture, we note that our model as written applies only to stalked daughter cells, in which case the FtsZ dynamics satisfies the general requirements. Interestingly, in slow-growing *E. coli*, FtsZ synthesis displays a cell-cycle dependence similar to that observed in *C. crescentus* swarmer cells [51]. A future extension of our framework to incorporate these similar additional layers of control could yield insights into their implications for cell-size homeostasis.

Alternatively, we may connect the identities in our model directly to the growth of cell surface, a complex process involving synthesis of PG precursors in the cytosol followed by final PG units at the cell surface [59]. The PG precursor synthesis is expected to occur in a cell-cycle-independent manner and has been proposed as a regulator between growth and division, with accumulation of excess PG precursor material serving as a potential checkpoint for constriction initiation [60]. Intriguingly, a mechanical homeostatic mechanism has been proposed to balance surface PG synthesis with overall cell growth rate [61]. In stalked *C. crescentus* cells, PG synthesis occurs in an FtsZ-dependent manner, leading to medial elongation prior to Z-ring formation and predominantly midcell constriction thereafter [36,62]. In *E. coli*, preseptal synthesis is less important to cell elongation [63], although a similar competition between elongation and constriction for PG synthesis has been reported [64]. In this picture, we may connect Q to a component of PG synthesis (such as nonseptal PG subunits), with Θ and T remaining the initiation of constriction and the interval between constriction initiation and cell division, respectively. The FtsZ dynamics then plays an essential role in controlling the onset of constriction, with the thresholded species Q connecting cell elongation to the cell division machinery via an unknown mechanism. Further experiments are needed to distinguish between these possibilities.

4. Stochastic behavior of T

We now consider stochasticity in the intergenerational evolution of size arising from the division process duration T. Inspired by the phenomenon of FtsZ treadmilling, in which it has been observed that divisome proteins follow treadmilling filaments by a diffusion-and-capture mechanism as the process of cell wall constriction occurs [65], we speculate that the constriction-controlled division process may be approximately modeled as one-dimensional drift combined with diffusion, where the traveling entity must traverse a certain distance to complete the process of division. (Perhaps the division machinery must move with the treadmilling FtsZ filaments around the Z ring a certain number of times.) In this scenario, T can be modeled as a first-passage time (FPT) for one-dimensional drift with diffusion, whose distribution is an inverse Gaussian [16,66]

$$P_{\mathrm{FPT}}(T) = \sqrt{\frac{\mathrm{Pe}\overline{T}}{2(T)^3}}\, e^{-\mathrm{Pe}(T-\overline{T})^2/2\overline{T}T}, \tag{25}$$

where Pe is the dimensionless Péclet number characterizing the drift-diffusion process and $\overline{T}$ is the mean FPT. (If the process involves drift velocity v, diffusion constant D, and traversal length ℓ, then the Péclet number $\mathrm{Pe} = \ell v/D$.) The experimentally determined T distribution along with its fit with an inverse Gaussian is shown in Fig. 6. From the fit,

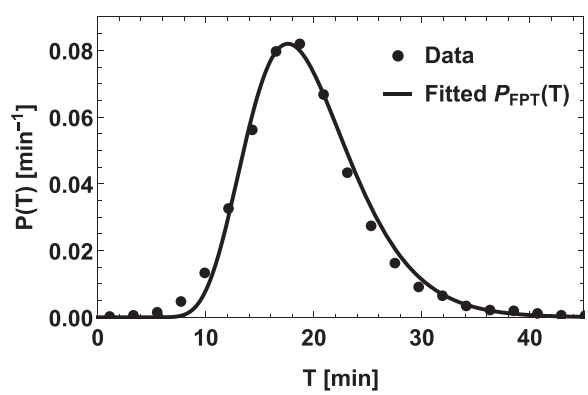

FIG. 6. Experimentally observed distribution of T, compared with an inverse Gaussian fit, with Eq. (25) corresponding to a FPT process involving one-dimensional diffusion and drift. The fit yields Péclet number $\mathrm{Pe} \approx 14$ and mean FPT $\overline{T} \approx 20$ min.

we deduce a rough estimate of the Péclet number Pe ≈ 14 governing the underlying process (mean FPT $\overline{T} \approx 20$ min).

III. CONCLUSION

Observations of single *C. crescentus* cells with genetically and chemically perturbed constriction rates have demonstrated a role for constriction rate in size control and homeostasis [67]. Future studies applying our framework to observations of single cells with perturbed constriction rates, i.e., modified T distributions, will yield further insights into the mechanism of stochastic intergenerational homeostasis under diverse conditions.

We have three primary reasons for not using previous models [68,69] and introducing the time delay T. First, *C. crescentus* does not follow adder, timer, or sizer models [3,18]. In our model, having nonzero T is essential for modeling *C. crescentus* cells since setting $T = 0$ results in adderlike behavior. Second, existing models (without T) do not explain the observed intergenerational scaling law that the conditional next generation's initial-size distribution given current generation's initial size, when rescaled by its mean value, results in an invariant distribution invariant of current generation's initial size. This scaling law is central to the stochastic intergenerational dynamics of cell-size homeostasis, as shown in [3,4]. Finally, we have identified FtsZ as a strong candidate for Q, and the recruitment of FtsZ to the division plane to initiate constriction as the thresholding process of Q. In this scenario, the time taken for constriction is represented by T.

The mechanistic scheme we have proposed here displays the common property of control systems that the set of parameter values that give rise to the same emergent dynamics [constrained by Eqs. (18) and (19)], though infinitely large, is vanishingly thin compared to the set of all possible parameter values. This point is underscored in Figs. 7, 8, and 9, which show that our predictions are robust irrespective of specific choice of model parameters within their permitted ranges. This allows for large situation-dependent variation in internal parameters while conserving the intergenerational size dynamics. In addition, preserving the constraints on certain protocols in our model allows for deconstraining other aspects of cellular processes while robustly maintaining cell-size homeostasis. As growth conditions and the quality of available nutrients change, different underlying molecular circuitry may be involved in condition specific ways. Thus, the net effect may be to alter the underlying stochastic Hinshelwood cycle and hence the rates k_X, k_Q, and k'_Q and also T. However, these alterations do not result in a breakdown of homeostasis since the homeostasis mechanism is indifferent to specific values of the rates of production of Q and X, provided the basic feature of initiation of division upon Q crossing the threshold is retained across conditions.

The data sets for constant growth conditions at 34 °C utilized in this paper are published in [8].

ACKNOWLEDGMENTS

R.R.B. and S.I.-B. gratefully acknowledge Purdue University Startup funds and the Purdue Research Foundation for supporting the collaboration and the research. S.I.-B. thanks the Purdue College of Science Dean's Special Fund and the Showalter Trust for partial support. K.J. and S.I.-B. acknowledge support from the Ross-Lynn Fellowship award and the Bilsland Dissertation Fellowship award. We are grateful to group members of S.I.-B. for useful discussions. R.R.B. and S.I.-B. thank Christine Jacobs-Wagner, Erin Goley, Jie Xiao, Suckjoon Jun, Sean Crosson, Marc Kirschner, and John Doyle for helpful discussions.

K.J., R.R.B., and S.I.-B. conceived of and designed the research; K.J. developed the theoretical framework under the guidance of S.I.-B.; K.J., R.R.B., and S.I.-B. performed analytic calculations; K.J. performed data analyses and simulations under the guidance of R.R.B. and S.I.-B.; C.S.W. made connections to molecular biological contexts with input from K.J. and S.I.-B.; K.J., C.S.W., R.R.B., and S.I.-B. wrote the paper; and S.I.-B. supervised the research.

The authors declare that they have no competing interests.

APPENDIX

1. Distribution of X when Q crosses the threshold

In the rescaled time coordinates [Eq. (7)], X and Q are decoupled [Eq. (8)]. Thus, the distribution of X_Θ (copy numbers of X when Q crosses threshold Θ) can be obtained by first finding the FPT of Q crossing the threshold and then finding the distribution of copy numbers of X at this FPT. The probability that this FPT lies between 0 and τ is equal to the probability that the value of Q at τ is greater than or equal to Θ,

$$\int_0^\tau P_\Theta(t)dt = \sum_\Theta^\infty P_Q(Q,\tau), \tag{A1}$$

where $P_\Theta(t)$ is the probability density that Q first crosses the threshold Θ at time t and $P_Q(Q,t)$ is the probability distribution of Q at time t. Differentiating with respect to τ,

$$P_\Theta(t) = -\sum_0^{\Theta-1} \frac{\partial P_Q(Q,t)}{\partial t}. \tag{A2}$$

Replacing the right-hand side using the master equation for Q given by

$$\frac{\partial P_Q(Q,t)}{\partial t} = P_Q(Q-1,t) - P_Q(Q,t), \tag{A3}$$

we obtain

$$P_\Theta(t) = P_Q(\Theta-1,t). \tag{A4}$$

The master equation for a simple birth process [Eq. (A3)], when solved using the method of characteristics on the generating function, gives the simple Poisson solution

$$P_Q(Q,t) = \frac{t^{Q-Q_i}e^{-t}}{(Q-Q_i)!}, \tag{A5}$$

where Q_i is the value of Q at birth ($t = 0$). Substituting this in Eq. (A4), we get

$$P_\Theta(t) = \frac{t^{\Theta-Q_i-1}e^{-t}}{(\Theta-Q_i-1)!}. \tag{A6}$$

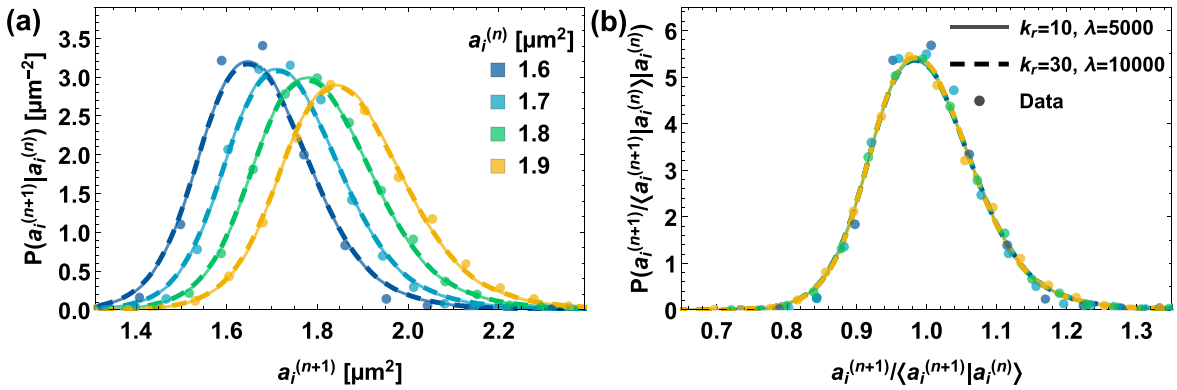

FIG. 7. Intergenerational scaling law, where model predictions robustly match experimental data irrespective of the exact choice of model parameters. (a) Conditional distributions of the next generation's initial areas $a_i^{(n+1)}$, given the current generation's initial areas $a_i^{(n)}$), plotted for four different current initial areas (marked by different colors). The solid lines are the results of exact model simulations with the parameters $k_r = 10$ and $\lambda = 5000$ μm^{-2} (same as Fig. 3), the dashed lines show simulation results with the parameters $k_r = 30$ and $\lambda = 10\,000$ μm^{-2}, and the points represent experimental data. (b) Both experimentally measured and theoretically calculated distributions in (a) overlap when rescaled by their respective mean values.

Now, similar to Eq. (A5), the solution for the simple birth process for X [Eq. (8)] is given by

$$P_X(X,t) = \frac{(k_r t)^{X-X_i} e^{-k_r t}}{(X-X_i)!}, \tag{A7}$$

where X_i is the initial value of X at birth ($t = 0$). Finally, the distribution of X_Θ (copy numbers of X when Q crosses threshold Θ) is given by

$$P_{X_\Theta}(X_\Theta) = \int_0^\infty P_X(X,t) P_\Theta(t) dt. \tag{A8}$$

Solving this equation by substituting Eqs. (A6) and (A7) results in Eq. (9).

2. Conditional moments of $X_\Theta^{(n+1)}$ given $X_\Theta^{(n)}$

a. Moments of X_Θ given X_i and Q_i

For a cell starting with initial copy numbers X_i and Q_i of X and Q, respectively, with the change of variables $\Delta Q = \Theta - Q_i$, the generating function corresponding to the probability distribution distribution in Eq. (9) is

$$G_\Theta(z|X_i, \Delta Q) = z^{X_i}[1 + k_r(1-z)]^{-\Delta Q}. \tag{A9}$$

To find the moments, first consider the operator $z\partial_z$ applied to the generating function

$$z\partial_z G_\Theta(z|X_i, \Delta Q) = X_i G_\Theta(z|X_i, \Delta Q) + k_r \Delta Q G_\Theta(z|X_i + 1, \Delta Q + 1). \tag{A10}$$

Thus, we can define the coefficients $C_{m,k}$ as

$$(z\partial_z)^m G_\Theta(z|X_i, \Delta Q) = \sum_{k=0}^{m} C_{m,k}(X_i, \Delta Q) \times G_\Theta(z|X_i + k, \Delta Q + k) \tag{A11}$$

such that

$$\langle X_\Theta^m | X_i, \Delta Q\rangle = \sum_{k=0}^{m} C_{m,k}(X_i, \Delta Q). \tag{A12}$$

Now consider two operators F_0 and F_1 such that

$$F_0 G_\Theta(z|a,b) = a G_\Theta(z|a,b), \tag{A13a}$$

$$F_1 G_\Theta(z|a,b) = k_r b G_\Theta(z|a+1, b+1). \tag{A13b}$$

Thus, F_0 leaves G_Θ unchanged, F_1 raises the index of G_Θ by 1, and

$$(z\partial_z)^m G_\Theta(z|X_i, \Delta Q) = (F_0 + F_1)^m G_\Theta(z|X_i, \Delta Q). \tag{A14}$$

The coefficient $C_{m,k}$ is determined by the sum of all permutations of different orderings of F_0 and F_1 applied to G_Θ such that there are a total k of F_1 and $m-k$ of F_0. Since F_0 does not change the index of G_Θ, the contribution to the coefficient from F_1's is fixed, independent of the ordering. The contribution of any F_0 depends only on how many F_1's came before it in that ordering. Denoting the positions of F_0's in a given ordering by p_i, we have

$$C_{m,k}(X_i, \Delta Q) = k_r^k \frac{(\Delta Q + k - 1)!}{(\Delta Q - 1)!} \times \sum_{1 \leqslant p_1 < p_2 < \cdots < p_{m-k} \leqslant m} \prod_j (X_i + p_j - j), \tag{A15}$$

where the term outside the summation is the contribution from the k F_1's, and the jth F_0 has $p_j - j$ F_1's before it in the ordering (a total of $p_j - 1$ operators before it, out of which $j-1$ are F_0's). Thus,

$$\langle X_\Theta^m | X_i, \Delta Q\rangle = \sum_{i=0}^{m} k_r^i \frac{(\Delta Q + i - 1)!}{(\Delta Q - 1)!} \times \sum_{1 \leqslant p_1 < p_2 < \cdots < p_{m-i} \leqslant m} \prod_{j=1}^{m-i} (X_i + p_j - j). \tag{A16}$$

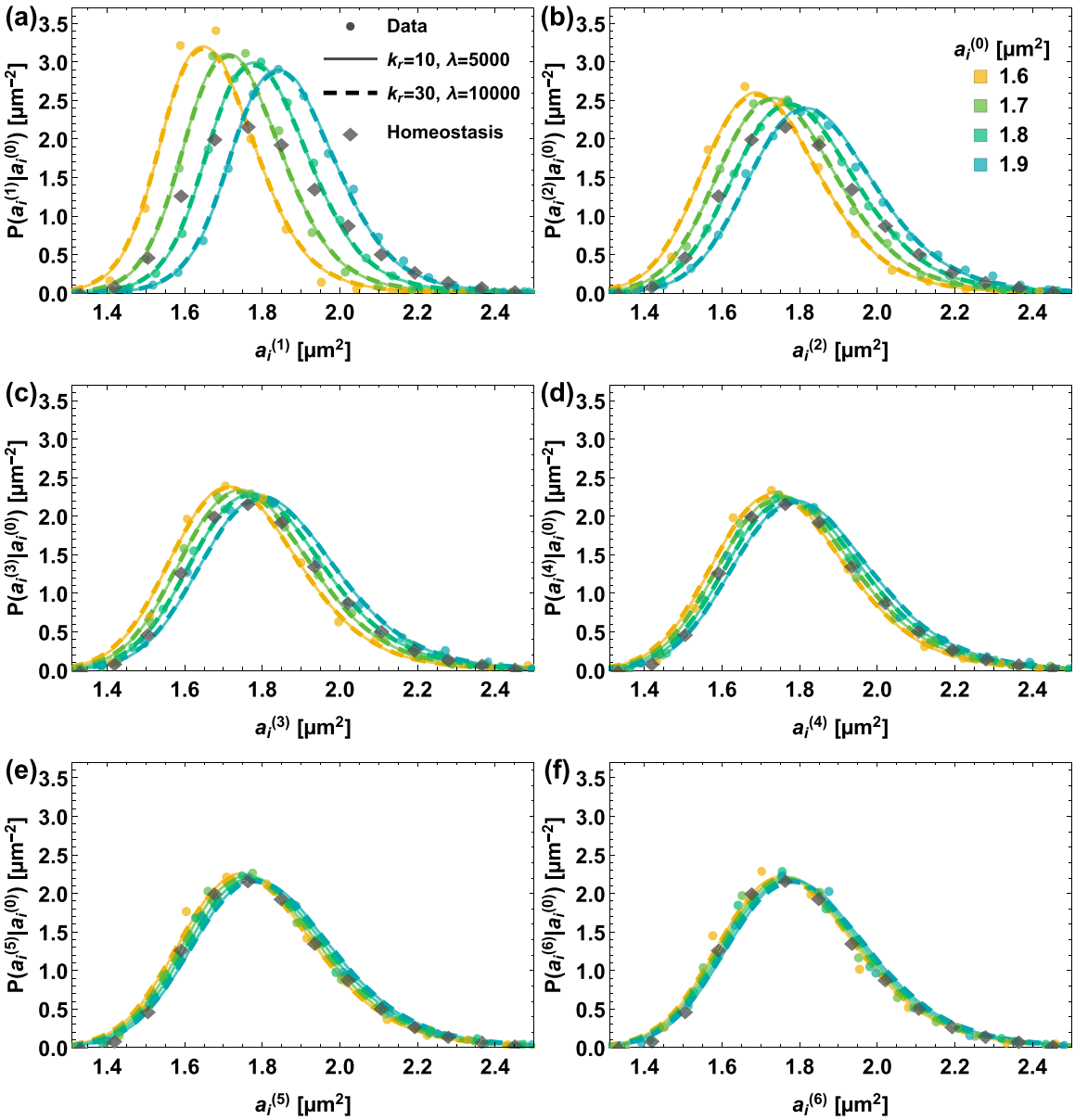

FIG. 8. Precision kinematics of stochastic intergenerational homeostasis, where model predictions robustly match experimental data irrespective of the exact choice of model parameters. The conditional distributions of initial sizes after n generations $a_i^{(n)}$, conditioned on the starting generation's initial size $a_i^{(0)}$, plotted for (a) $n = 1$, (b) $n = 2$, (c) $n = 3$, (d) $n = 4$, (e) $n = 5$, and (f) $n = 6$. The four different starting initial areas $a_i^{(0)}$ correspond to different colors. The solid lines are theoretical predictions based on exact simulations of the mechanistic model with the parameters $k_r = 10$ and $\lambda = 5000$ μm^{-2} (same as Fig. 4), the dashed lines are theoretical predictions with the parameters $k_r = 30$ and $\lambda = 10\,000$ μm^{-2}, and the points are experimentally measured data. The diamonds denote the experimentally measured populationwide homeostatic initial area distribution.

Keeping only the leading powers of X_i and ΔQ gives us

$$\langle X_\Theta^m | X_i, \Delta Q\rangle = \sum_{i=0}^{m} k_r^i [\Delta Q^i + o(\Delta Q^{i-1})] \times \left[\binom{m}{m-i} X_i^{m-i} + o\big(X_i^{m-i-1}\big)\right]. \quad \text{(A17)}$$

b. Joint moments of X_f and Q_f given X_Θ

After Q crosses the threshold, starting from copy numbers X_Θ and Θ of X and Q, respectively, here we first find the joint generating function of their copy numbers at the time of division, X_f and Q_f. Division occurs at time T after the crossing of the threshold (which we mark as $t = 0$ for this section), following reactions given by Eqs. (1) and (6) with modified post-threshold rate k'_Q instead of k_Q. For this problem, we cannot decouple the reactions using the equivalence method anymore, because time is involved. The master equation for these reactions is

$$\frac{\partial P(X, Q, t)}{\partial t} = k_X (X-1) P(X-1, Q, t) + k'_Q X P(X, Q-1, t) - (k_X + k'_Q) X P(X, Q, t). \quad \text{(A18)}$$

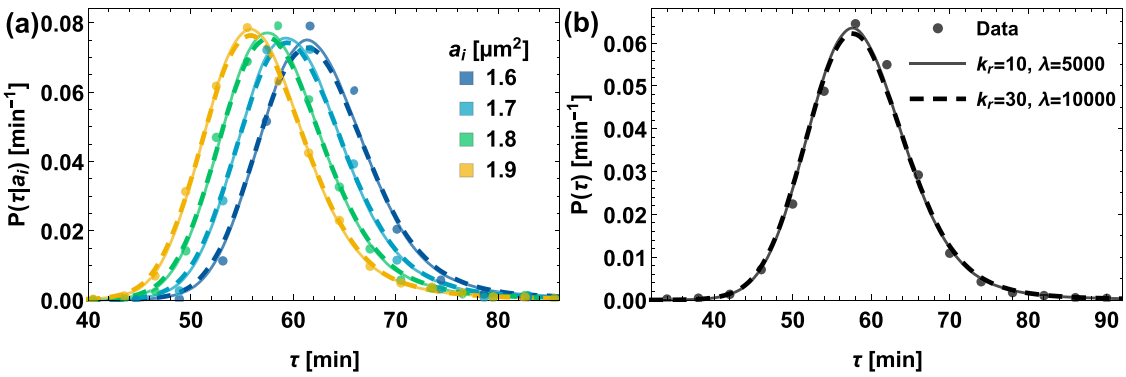

FIG. 9. Shape of the interdivision time distribution, where model predictions robustly match experimental data irrespective of the exact choice of model parameters. (a) Division time distributions disambiguated by initial area plotted for different initial areas (distinguished by different colors). (b) Full division time distribution. The solid lines are theoretical predictions based on exact simulations of the mechanistic model with the parameters $k_r = 10$ and $\lambda = 5000\ \mu\text{m}^{-2}$ (same as Fig. 5), the dashed lines are theoretical predictions with the parameters $k_r = 30$ and $\lambda = 10\,000\ \mu\text{m}^{-2}$, and the points are experimentally measured steady-state data.

We convert this to a differential equation for the generating function instead, using the transformation

$$G(z_x, z_q, t) = \sum_{X,Q} z_x^X z_q^Q P(X, Q, t). \tag{A19}$$

Thus,

$$\partial_t G = k_X z_x^2 \partial_{z_x} G + k'_Q z_x z_q \partial_{z_x} G - (k_X + k'_Q) z_x \partial_{z_x} G. \tag{A20}$$

Solving this through the method of characteristics and setting $t = T$, we get the joint generating function of X_f and Q_f,

$$G(z_x, z_q|X_\Theta) = z_x^{X_\Theta} f_q^{X_\Theta} z_q^{\Theta} [f_q e^{f_q T} + k_X(1 - e^{f_q T}) z_x]^{-X_\Theta}, \tag{A21a}$$

$$f_q \equiv k_X + k'_Q(1 - z_q). \tag{A21b}$$

Now, proceeding similarly to the method in Appendix 2 a, we get

$$\begin{aligned}(z_x\partial_{z_x})^m G(z_x, z_q|X_\Theta) &= \sum_{i=0}^{m} \frac{(X_\Theta + i - 1)!}{(X_\Theta - 1)!} k_X^i \left(\frac{e^{f_q T} - 1}{f_q}\right)^i G(z_x, z_q|X_\Theta + i) \\ &\times \sum_{1\leqslant p_1<p_2<\cdots<p_{m-i}\leqslant m} \prod_{j=1}^{m-i} (X_\Theta + p_j - j).\end{aligned} \tag{A22}$$

Now we can take the limit $z_x = 1$,

$$\begin{aligned}(z_x\partial_{z_x})^m G(z_x, z_q|X_\Theta)|_{z_x=1} &= \sum_{i=0}^{m} \frac{(X_\Theta + i - 1)!}{(X_\Theta - 1)!} k_X^i \left(\frac{e^{f_q T} - 1}{f_q}\right)^i G(1, z_q|X_\Theta + i) \\ &\times \sum_{1\leqslant p_1<p_2<\cdots<p_{m-i}\leqslant m} \prod_{j=1}^{m-i} (X_\Theta + p_j - j).\end{aligned} \tag{A23}$$

We have

$$\langle X_f^{m_x} Q_f^{m_q} | X_\Theta \rangle = (z_q\partial_{z_q})^{m_q} \left[\left(z_x\partial_{z_x}\right)^{m_x} G(z_x, z_q|X_\Theta)|_{z_x=1} \right]|_{z_q=1}. \tag{A24}$$

Thus, we need to find $(z_q\partial_{z_q})^m (\frac{e^{f_q T}-1}{f_q})^i G(1, z_q|X_\Theta + i)$. First, consider an expression of the form $(z\partial_z)^m u(z)[v(z)]^{-X}|_{z=1}$ such that $v(1) = 1$. To get the coefficient of largest power of X, each time we differentiate by parts, we only do so to the $[v(z)]^{-X}$ term and ignore all other terms. Thus, the term with the leading coefficient is

$$(-1)^m \frac{(X + m - 1)!}{(X - 1)!} [v(z)]^{-X-m} [\partial_z v(z)]^m u(z) z^m. \tag{A25}$$

Thus, the largest power of X is m and the coefficient of X^m at $z = 1$ is,

$$u(1)[-\partial_z v(z)|_{z=1}]^m. \tag{A26}$$

Applying this to our system, the coefficient largest power of X_Θ (X_Θ^m) in $(z_q\partial_{z_q})^m (\frac{e^{f_q T}-1}{f_q})^i G(1, z_q|X_\Theta + i)$ is $(k'_Q)^m [\frac{e^{k_X T}-1}{k_X}]^{m+i}$. Inserting this back into Eq. (A24),

$$\begin{aligned}\langle X_f^{m_x} Q_f^{m_q} | X_\Theta \rangle &= e^{m_x k_X T} \left[\frac{k'_Q}{k_X}(e^{k_X T} - 1)\right]^{m_q} X_\Theta^{m_x + m_q} \\ &+ o\left(X_\Theta^{m_x + m_q - 1}\right).\end{aligned} \tag{A27}$$

c. Incorporating the division rule

Applying the division rule given by Eq. (10) to Eq. (A17),

$$\begin{aligned}\langle (X_\Theta^{(n+1)})^m | X_f^{(n)}, Q_f^{(n)} \rangle &= \sum_{i=0}^{m} \left(k_r^{(n+1)}\right)^i \left[(-r^{(n)})^i \left(Q_f^{(n)}\right)^i + o\left(\left[Q_f^{(n)}\right]^{i-1}\right)\right] \\ &\times \left[\binom{m}{i} (r^{(n)})^{m-i} \left(X_f^{(n)}\right)^{m-i} + o\left(\left[X_f^{(n)}\right]^{m-i-1}\right)\right].\end{aligned} \tag{A28}$$

Combining with Eq. (A27), we get

$$\left\langle \left(X_\Theta^{(n+1)}\right)^m \middle| X_\Theta^{(n)} \right\rangle = \sum_{j=0}^{m} c_{j;m}^{(n)} \left(X_\Theta^{(n)}\right)^j, \tag{A29a}$$

$$\begin{aligned} c_{m;m}^{(n)} &= \left(r^{(n)} \left[e^{k_X^{(n)} T^{(n)}} - \frac{k_Q'^{(n)}}{k_X^{(n)}} k_r^{(n+1)} (e^{k_X^{(n)} T^{(n)}} - 1) \right] \right)^m \\ &\equiv [A^{(n)}]^m, \end{aligned} \tag{A29b}$$

where $c_{j;m}$'s are finite functions of k_X, k_Q, k_Q', Θ, and r, which are all finite positive stochastic variables (except k_Q', which is finite and non-negative).

3. Necessary and sufficient condition for cell-size homeostasis

For cell size to be in homeostasis, starting from any given $X_\Theta^{(0)}$, $\overline{\langle (X_\Theta^{(n+1)})^m | X_\Theta^{(0)} \rangle}$ should tend to the same finite value as n tends to infinity irrespective of the starting $X_\Theta^{(0)}$ value. Here the overline represents averaging over the ensemble of k_X, k_Q, k_Q', Θ, and r values.

a. Forgetting the initial condition

One of the conditions for cell size to be in homeostasis is that $\langle (X_\Theta^{(n+1)})^m | X_\Theta^{(0)} \rangle$ should not depend on X_Θ as n tends to ∞. From Eq. (A29),

$$\left\langle \left(X_\Theta^{(n+1)}\right)^m \middle| X_\Theta^{(n)} \right\rangle = [A^{(n)}]^m \left(X_\Theta^{(n)}\right)^m + o\left(\left(X_\Theta^{(n)}\right)^{m-1}\right). \tag{A30}$$

Continuing the expansion of the above series, we get

$$\overline{\left\langle \left(X_\Theta^{(n+1)}\right)^m \middle| X_\Theta^{(0)} \right\rangle} = \overline{\left[\prod_{k=0}^{n} A^{(k)} \right]^m} \left(X_\Theta^{(0)}\right)^m + o\left(\left(X_\Theta^{(0)}\right)^{m-1}\right), \tag{A31}$$

where the overline represents averaging over the ensemble of all possible values of $A^{(k)}$. Thus, for the dependence on $X_\Theta^{(0)}$ to vanish as n tends to ∞, it is necessary to have

$$\lim_{n\to\infty} \overline{\left[\prod_{k=0}^{n} A^{(k)} \right]^m} = 0. \tag{A32}$$

To simplify the calculation, we assume all $A^{(j)}$'s are independent and identically distributed variables. This requires all variables r, k_X, k_Q', k_r, and T in any given generation to not depend on their values in the previous generation and for k_r to be independent of other variables even within the same generation. Here $k_Q = k_X/k_r$; thus we are requiring that k_Q and k_X are correlated, but k_r is independent. Under these assumptions, the above relation can be rewritten as

$$\lim_{n\to\infty} a_m^n = 0, \tag{A33}$$

where a_m is the mth moment of A, and the above relation must be satisfied for all moments. Thus, $|a_m| < 1\,\forall\, m$ is a necessary condition for cell-size homeostasis. In [4] we show that this condition is equivalent to saying that the maximum possible value of A is less than or equal to 1, unless A is Dirac δ distributed (in which case, the maximum possible value is strictly less than 1). Next we prove that this condition is also sufficient for $\overline{\langle (X_\Theta^{(n)})^m | X_\Theta^{(0)} \rangle}$ to tend to the same finite value as n tends to infinity irrespective of the starting $X_\Theta^{(0)}$ value, for all moments m, through the principle of mathematical induction.

b. Convergence of the first moment

Substituting $m = 1$ in Eq. (A16),

$$\langle X_\Theta | X_i, \Delta Q \rangle = X_i + k_r \Delta Q. \tag{A34}$$

Substituting $m = 1$ in Eq. (A23),

$$\begin{aligned} &z_x \partial_{z_x} G(z_x, z_q | X_\Theta)|_{z_x=1} \\ &\quad = G(1, z_q | X_\Theta) X_\Theta + X_\Theta k_X \left(\frac{e^{f_q T} - 1}{f_q} \right) G(1, z_q | X_\Theta + 1). \end{aligned} \tag{A35}$$

Now, from Eq. (A24),

$$\begin{aligned} \langle X_f | X_\Theta \rangle &= [(z_x \partial_{z_x}) G(z_x, z_q | X_\Theta)|_{z_x=1}]|_{z_q=1} \\ &= e^{k_X T} X_\Theta, \end{aligned} \tag{A36a}$$

$$\begin{aligned} \langle Q_f | X_\Theta \rangle &= z_q \partial_{z_q} G(1, z_q | X_\Theta)|_{z_q=1} \\ &= \Theta + \frac{k_Q'}{k_X} (e^{k_X T} - 1) X_\Theta. \end{aligned} \tag{A36b}$$

Combining the above equations with Eq. (A34) using the division rules [Eq. (10)],

$$\left\langle X_\Theta^{(1)} \middle| X_\Theta \right\rangle = r e^{k_X T} \left[1 - \frac{k_Q'}{k_X} k_r^{(1)} (1 - e^{-k_X T}) \right] X_\Theta + k_r^{(1)} \frac{\Theta}{2}. \tag{A37}$$

Defining M_1 as the maximum possible value of $k_r^{(1)} \frac{\Theta}{2}$, consider the stochastic map

$$x_{n+1} = A^{(n)} x_n + M_1, \tag{A38}$$

with $x_0 = X_\Theta^{(0)}$. If the above series converges to a finite value as n tends to ∞, $\langle X_\Theta^{(n)} | X_\Theta^{(0)} \rangle$ will also converge due to the relation

$$\left\langle X_\Theta^{(n)} \middle| X_\Theta^{(0)} \right\rangle \leqslant x_n \,\forall\, n, \tag{A39}$$

from the definition of M_1. By continuing to expand the series to x_0 and taking the ensemble average over A values, we get

$$\overline{x_{n+1}} = a_1^{n+1} x_0 + M_1 \sum_{j=1}^{n} a_1^j. \tag{A40}$$

Since we have the condition $|a_1| < 1$, the above converges to the finite value $M_1/(1-a_1)$ as $n \to \infty$. Thus, $\overline{\langle X_\Theta^{(n)}|X_\Theta^{(0)}\rangle}$ also converges to a finite value. Furthermore, the largest power of $X_\Theta^{(0)}$ in $\overline{\langle X_\Theta^{(n)}|X_\Theta^{(0)}\rangle}$ is 1, and in the previous section we have already shown that the coefficient of leading power goes to 0 as n tends to ∞ and thus $\overline{\langle X_\Theta^{(n)}|X_\Theta^{(0)}\rangle}$ becomes independent of $X_\Theta^{(0)}$.

c. Convergence of higher moments

Here we prove the necessary condition $|a_m| < 1\,\forall\, m$ is also sufficient through the principle of mathematical induction. We have already proved that this condition is sufficient for the convergence to a finite initial-condition-independent value of the first moment $m = 1$. Next, assuming it is sufficient for all moments $m = 1$ to k, we need to show that it must also be sufficient for $m = k+1$. Thus, as n tends to ∞, $\langle (X_\Theta^{(n)})^j|X_\Theta^{(0)}\rangle$ for $j \leqslant k$ all tend to their finite steady-state values, say, y_j, that are independent of $X_\Theta^{(0)}$. From Eq. (A29),

$$\lim_{n\to\infty}\left\langle (X_\Theta^{(n+1)})^{k+1}\middle|X_\Theta^{(0)}\right\rangle = \lim_{n\to\infty}(A^{(n)})^{k+1}\left\langle \left(X_\Theta^{(n)}\right)^{k+1}\middle|X_\Theta^{(0)}\right\rangle + \sum_{j=0}^{k} c_{j;k+1}^{(n)} y_j. \quad \text{(A41)}$$

Now consider the series

$$z_{n+1} = (A^{(n)})^{k+1} z_n + \sum_{j=0}^{k} c_{j;k+1} y_j, \quad \text{(A42)}$$

with some arbitrary initial condition z_0, where $c_{j;k+1}$ are the maximum possible values of $c_{j;k+1}^{(n)}$. If this series converges to the same finite value independent of z_0, $\lim_{n\to\infty}\langle (X_\Theta^{(n)})^{k+1}|X_\Theta^{(0)}\rangle$ also converges to that value due to Eq. (A41). First, consider that since there are finite terms in the summation and each term is finite, the summation term has a finite upper bound, say, M_{k+1}. Then consider the series

$$x_{n+1} = (A^{(n)})^{k+1} x_n + M_{k+1}, \quad \text{(A43)}$$

with the initial condition $x_0 = z_0$. This satisfies

$$z_n \leqslant x_n\,\forall\, n. \quad \text{(A44)}$$

Thus, if x_n converges to a finite value as n tends to ∞, z_n must converge to a finite value too. By further expanding the series to x_0 and taking the ensemble average over A values we get

$$\overline{x_{n+1}} = a_{k+1}^{n+1} x_0 + M_{k+1}\sum_{j=1}^{n} a_{k+1}^{j}. \quad \text{(A45)}$$

Since we have the condition $|a_{k+1}| < 1$, the above converges to the finite value $M_{k+1}/(1-a_{k+1})$ as $n \to \infty$. Thus, z_n also converges to a finite value that is less than or equal to this value. Next, expanding the series for z_{n+1} [Eq. (A42)] until z_0 and taking the ensemble average over A values, we find that the only term containing z_0 is $a_{k+1}^{n+1} z_0$, which goes to zero as n tends to ∞ when $|a_{k+1}| < 1$. Thus, $\overline{z_n}$ tends to a finite value independent of z_0 and hence $\overline{\langle (X_\Theta^{(n)})^{k+1}|X_\Theta^{(0)}\rangle}$ also tends to a finite value independent of $X_\Theta^{(0)}$, thus completing the proof.

4. Quasideterministic limit

In the quasideterministic limit, the copy numbers of X and Q are considered large enough such that the reactions given by Eqs. (1) and (6) proceed deterministically for a given cell cycle. Thus, the primary source of noise in the system is due to the intergenerational variation of reaction rates k_X, k_Q, and k'_Q, as well as the time between the crossing of threshold and division T.

a. Conditional moments of X_Θ

Consider the smaller conditional moments of X_Θ in the limit that the copy numbers of X and Q are large, i.e., $X_i, \Delta Q \gg m \geqslant 1$. In Eq. (A16), setting $X_i + p_j - j \approx X_i$ etc.,

$$\left\langle X_\Theta^m\middle|X_i, \Delta Q\right\rangle \approx \sum_{i=0}^{m} k_r^i n^i \binom{m}{m-i} X_i^{m-i} = (X_i + k_r\Delta Q)^m. \quad \text{(A46)}$$

Applying the division rules [Eq. (10)] to the above,

$$\left\langle \left(X_\Theta^{(n+1)}\right)^m\middle|X_f^{(n)}, Q_f^{(n)}\right\rangle \approx \left[r^{(n)}X_f^{(n)} + k_r^{(n+1)}\left(\left(\tfrac{1}{2} + r^{(n)}\right)\Theta - r^{(n)}Q_f^{(n)}\right)\right]^m. \quad \text{(A47)}$$

Next, in order to find joint moments of X_f and Q_f given X_Θ by solving Eq. (A24) using Eq. (A23), first consider

$$z_q\partial_{z_q}\left(\frac{e^{f_qT}-1}{f_q}\right)^i G(1, z_q|X_\Theta + i) = z_q\partial_{z_q}(e^{[k_X+k'_Q(1-z_q)]T} - 1)^i z_q^\Theta [k_X + k'_Q(1-z)]^X \times [k_X + k'_Q(1-z_q)e^{[k_X+k'_Q(1-z_q)]T}]^{-X-i}. \quad \text{(A48)}$$

Consider $(z\partial_z)^m u(z) z^\Theta [v(z)]^{-X_\Theta}|_{z=1}$ such that $v(1) = 1$. Since $X_\Theta^2 \gg X_\Theta$ and $\Theta^2 \gg \Theta$, all other terms are insignificant compared to the terms with highest powers of X_Θ and Θ added. First,

$$z\partial_z u(z) z^\Theta [v(z)]^{-X_\Theta}|_{z=1} \approx u(1)\{\Theta z^\Theta [v(z)]^{-X_\Theta} - X_\Theta [v(z)]^{-X_\Theta-1}[\partial_z v(z)]\}|_{z=1}. \quad \text{(A49)}$$

Now, since we are keeping only the highest powers of X_Θ and Θ added, we will not further differentiate $\partial_z v(z)$ on subsequent steps (since it would result in terms with lower powers of X_Θ), treating it as a constant. Thus,

$$\begin{aligned}(z\partial_z)^m u(z) z^\Theta [v(z)]^{-X_\Theta}|_{z=1} &\approx u(1)\sum_{i=1}^{m}\frac{(X_\Theta + i - 1)!}{(X_\Theta - 1)!}[-\partial_z v(z)|_{z=1}]^i \binom{m}{i}\Theta^{m-i}\\ &\approx u(1)\sum_{i=1}^{m} X_\Theta^i [-\partial_z v(z)|_{z=1}]^i \binom{m}{i}\Theta^{m-i}\\ &= u(1)[\Theta - \partial_z v(z)|_{z=1} X_\Theta]^m. \end{aligned} \quad \text{(A50)}$$

Applying this to our problem, we get

$$\begin{aligned}\langle X_f^{m_x} Q_f^{m_q} | X_\Theta \rangle &\approx \sum_{i=0}^{m_x} \frac{(X_\Theta + i - 1)!}{(X_\Theta - 1)!} (e^{k_X T} - 1)^i \left(\Theta + \frac{k'_Q (e^{k_X T} - 1)}{k_X} X_\Theta\right)^{m_q} \sum_{1 \leqslant p_1 < p_2 < \cdots < p_{m_x - i} \leqslant m_x} \prod_{j=1}^{m_x - i} (X_\Theta + p_j - j) \\ &\approx \sum_{i=0}^{m_x} X_\Theta^i (e^{k_X T} - 1)^i \left(\Theta + \frac{k'_Q (e^{k_X T} - 1)}{k_X} X_\Theta\right)^{m_q} \binom{m_x}{m_x - i} X_\Theta^{m_x - i} \\ &= e^{m_x k_X T} X_\Theta^{m_x} \left(\Theta + \frac{k'_Q (e^{k_X T} - 1)}{k_X} X_\Theta\right)^{m_q}. \end{aligned} \tag{A51}$$

Thus, in Eq. (A47), expanding in powers of X_f and Q_f and then replacing X_f by $e^{k_X T} X_\Theta$ and Q_f by $\Theta + \frac{k'_Q (e^{k_X T} - 1)}{k_X} X_\Theta$ and recombining, we get

$$\langle (X_\Theta^{(n+1)})^m | X_\Theta^{(n)} \rangle \approx \left(A^{(n)} X_\Theta^{(n)} + \frac{k_r^{(n+1)} \Theta}{2}\right)^m \forall\, m \ll X_\Theta, \Theta, \tag{A52}$$

where A is as defined in Eq. (A29).

b. Variation of $X_f^{(n)}$ and $X_i^{(n+1)}$ with $X_i^{(n)}$

From Eq. (A51),

$$X_f = e^{k_X T} X_\Theta. \tag{A53}$$

Applying the division rule [Eq. (10)],

$$X_i^{(n)} = r^{(n-1)} e^{k_X^{(n-1)} T^{(n-1)}} X_\Theta^{(n-1)}. \tag{A54}$$

Also, from Eqs. (A53) and (A52),

$$X_f^{(n)} = e^{k_X^{(n)} T^{(n)}} \left(A^{(n-1)} X_\Theta^{(n-1)} + \frac{k_r^{(n)} \Theta}{2}\right). \tag{A55}$$

Replacing X_Θ from Eq. (A54),

$$X_f^{(n)} = e^{k_X^{(n)} T^{(n)}} \left[1 - \frac{k_Q'^{(n-1)}}{k_X^{(n-1)}} k_r^{(n)} \left(1 - e^{-k_X^{(n-1)} T^{(n-1)}}\right)\right] X_i^{(n)} + e^{k_X^{(n)} T^{(n)}} \frac{k_r^{(n)} \Theta}{2}. \tag{A56}$$

Next, using the division rule (10),

$$X_i^{(n+1)} = r^{(n)} e^{k_X^{(n)} T^{(n)}} \left[\frac{k_r^{(n)} \Theta}{2} + \left(1 - \frac{k_Q'^{(n-1)}}{k_X^{(n-1)}} k_r^{(n)} \left(1 - e^{-k_X^{(n-1)} T^{(n-1)}}\right)\right) X_i^{(n)}\right]. \tag{A57}$$

c. Emergent simplicity: Scaling collapse of conditional initial-size distributions

If and only if rescaling the conditional next generation's initial-size distribution given the current generation's initial size results in a distribution invariant of the current generation's initial size, the stochastic map takes the form [4]

$$a_i^{(n+1)} = s^n \mu(a_i^n), \tag{A58}$$

where a_i is the initial size (size at birth), μ is a deterministic function, and $s^{(n)}$'s are independent and identically distributed stochastic variables. If we are to write Eq. (A57) in this form, the stochastic part of both the coefficient of X_i and the constant on the right-hand side must be the same and must be independent and identically distributed across generations. This is true when (i) $k'_Q = 0$; (ii) the rates k_X and k_Q are proportional, i.e., they both have noise but their ratio is constant k_r; and (iii) Θ has negligible noise. If these conditions are satisfied,

$$X_i^{(n+1)} = r^{(n)} e^{k_X^{(n)} T^{(n)}} \left[X_i^{(n)} + \tfrac{1}{2} k_r \Theta\right]. \tag{A59}$$

This results in the stochastic map given by Eqs. (15) and (17). Thus, the invariant mean-rescaled distribution of the next generation's initial sizes given the current generation's initial size is given by

$$P_s(s) = \iiint dr\, dk_X dT\, P_{r,k_X,T}(\overline{re^{k_X T}}, k_X, T) \delta\left(s - \frac{re^{k_X T}}{\overline{re^{k_X T}}}\right), \tag{A60}$$

where the overline denotes an intergenerational average and $P_{r,k_X,T}$ is the joint distribution of r, k_X, and T.

5. Alternate division rules

a. A constant amount of Q is split evenly and the rest is split according to division ratio

Consider a general alternative to Eq. (10),

$$Q_i^{(n+1)} = \frac{C}{2} + r^{(n)}\left[Q_f^{(n)} - C\right], \tag{A61}$$

where a constant C amount of Q_f is divided equally among the daughter cells at division and the remainder is divided according to the size division ratio r. Here, for consistency, C must not be greater than the minimum possible value of Q_f, which is Θ. Thus, $C \leqslant \Theta$. First, consider the effect on cell-size homeostasis. Since the coefficient of Q_f remains the same irrespective of C, Eq. (A28) does not change, and hence the necessary and sufficient condition for cell-size homeostasis [given by Eq. (12)] remains the same.

Next consider the dynamics in the quasideterministic limit. Applying the new division rule to Eq. (A47), Eq. (A52) now results in

$$X_\Theta^{(n+1)} = A^{(n)} X_\Theta^{(n)} + k_r^{(n+1)}\left[\Theta - \frac{C}{2} + r^{(n)}(C - \Theta)\right]. \tag{A62}$$

Thus, Eq. (A57) becomes

$$X_i^{(n+1)} = r^{(n)} e^{k_X^{(n)} T^{(n)}}\left(k_r^{(n)}\left[\Theta - \frac{C}{2} + r^{(n-1)}(C - \Theta)\right] + \left[1 - \frac{k_Q'^{(n-1)}}{k_X^{(n-1)}} k_r^{(n)}(1 - e^{-k_X^{(n-1)} T^{(n-1)}})\right] X_i^{(n)}\right). \tag{A63}$$

The constraint of mean rescaling of the distribution of $X_i^{(n+1)}$ given $X_i^{(n)}$ requires the stochastic part of both terms to be proportional in order to express the above equation in the form given by Eq. (A58). Thus, $k_Q' = 0$, k_r is constant, and $C = \Theta$. Thus, the division rule with $C = \Theta$ in Eq. (10) is not required to maintain cell-size homeostasis, but is needed for the mean rescaling of conditional initial-size distributions.

b. All of Q is split evenly

Consider another alternative to Eq. (10),

$$Q_i^{(n+1)} = \frac{Q_f^{(n)}}{2}, \tag{A64}$$

where all of Q_f is divided equally among the daughter cells at division. Applying this altered division rule to Eq. (A17), Eq. (A28) now becomes

$$\left\langle \left(X_\Theta^{(n+1)}\right)^m \middle| X_f^{(n)}, Q_f^{(n)} \right\rangle = \sum_{i=0}^{m} \left(k_r^{(n+1)}\right)^i \left\{2^{-i}\left(Q_f^{(n)}\right)^i + o\left(\left[Q_f^{(n)}\right]^{i-1}\right)\right\} \times \left[\binom{m}{i}(r^{(n)})^{m-i}(X_f^{(n)})^{m-i} + o([X_f^{(n)}]^{m-i-1})\right]. \tag{A65}$$

Combining with Eq. (A27), Eq. (A29) is modified to

$$\left\langle \left(X_\Theta^{(n+1)}\right)^m \middle| X_\Theta^{(n)} \right\rangle = \sum_{j=0}^{m} c_{j;m}'^{(n)} \left(X_\Theta^{(n)}\right)^j, \tag{A66a}$$

$$c_{m;m}'^{(n)} = r^{(n)} e^{k_X^{(n)} T^{(n)}} - \frac{k_r^{(n+1)} k_Q'^{(n)}}{2k_X^{(n)}}\left(e^{k_X^{(n)} T^{(n)}} - 1\right) \equiv A'^{(n)}. \tag{A66b}$$

The rest of the derivation of the necessary and sufficient condition for cell-size homeostasis does not change. Thus, the necessary and sufficient condition is still given by Eq. (12), except that A is replaced by A' as defined above.

Next consider the dynamics in the quasideterministic limit. Applying the new division rule to Eq. (A47), Eq. (A52) now results in

$$X_\Theta^{(n+1)} = A'^{(n)} X_\Theta^{(n)} + k_r^{(n+1)} \frac{\Theta}{2}. \tag{A67}$$

Thus, Eq. (A57) becomes

$$X_i^{(n+1)} = r^{(n)} e^{k_X^{(n)} T^{(n)}}\left[\frac{k_r^{(n)}\Theta}{2} + \left(1 - \frac{k_r^{(n)}}{2r^{(n-1)}} \frac{k_Q'^{(n-1)}}{k_X^{(n-1)}}\left(1 - e^{-k_X^{(n-1)} T^{(n-1)}}\right)\right) X_i^{(n)}\right]. \tag{A68}$$

The constraint of mean rescaling of the distribution of $X_i^{(n+1)}$ given $X_i^{(n)}$ requires the stochastic part of both terms to be proportional in order to express the above equation in the form given by Eq. (A58). Thus, $k_Q' = 0$ and k_r is constant. Note that for the special case $k_Q' = 0$, this alternate division rule given by Eq. (A64) is exactly identical to the original division rule [Eq. (10)] because $Q_f = \Theta$.

6. Exact solution for $k_Q' = 0$

For $k_Q' = 0$, we have $Q_i = \Delta Q = \Theta/2$ and $Q_f = \Theta$. Setting $\Delta Q = \Theta/2$ in Eq. (9),

$$P_{X_\Theta}(X_\Theta|X_i) = \binom{X_\Theta - X_i + \Theta/2 - 1}{\Theta/2 - 1}\left[\frac{k_r}{1 + k_r}\right]^{X_\Theta - X_i}\left[\frac{1}{1 + k_r}\right]^{\Theta/2}, \tag{A69}$$

where $X_\Theta \geqslant X_i$. Thus, $X_\Theta = X_i + \xi_0$, where ξ_0 is drawn from a Pascal distribution with the parameters $\Theta/2$ and $1/(1 + k_r)$. Next, setting $k_Q' = 0$ in Eq. (A21), the generating function of X_f given X_Θ is

$$G(z, t) = z^{X_\Theta} e^{-X_\Theta k_X t}[1 - (1 - e^{-k_X t})z]^{-X_\Theta}. \tag{A70}$$

From this generating function, we get the conditional distribution of X_f given X_Θ,

$$P_{f;\Theta}(X_f|X_\Theta) = \binom{X_f - 1}{X_\Theta - 1}(1 - e^{-k_X T})^{X_f - X_\Theta} e^{-X_\Theta k_X T}, \tag{A71}$$

for $X_f \geqslant X_\Theta$. Thus, $X_f = X_\Theta + \xi$, where ξ is drawn from a Pascal distribution with the parameters X_Θ and $e^{-k_X T}$.

Combining this with Eq. (A69), the distribution of X_f given X_i is

$$P_f(X_f|X_i) = \sum_{x=X_i}^{X_f} \binom{X_f-1}{x-1}(1-e^{-k_X T})^{X_f-x}e^{-xk_X T} \times \binom{x-X_i+\Theta/2-1}{\Theta/2-1}\left[\frac{k_r}{1+k_r}\right]^{x-X_i}\left[\frac{1}{1+k_r}\right]^{\Theta/2}. \tag{A72}$$

Using the properties of Pascal distributions, from Eq. (A69),

$$\langle X_f|X_\Theta\rangle = X_\Theta e^{k_X T}. \tag{A73}$$

Applying this to Eq. (A71),

$$\langle X_f|X_i\rangle = e^{k_X T}\left(X_i + \frac{k_r\Theta}{2}\right). \tag{A74}$$

Rewriting the above equation in terms of cell size instead of copy numbers by scaling X by $1/\lambda$, and taking the intergenerational average,

$$\overline{\langle a_f|a_i\rangle} = \overline{e^{k_X T}}\left(a_i + \frac{k_r\Theta}{2\lambda}\right), \tag{A75a}$$

$$\overline{\langle a_i^{(n+1)}|a_i^{(n)}\rangle} = \overline{re^{k_X T}}\left(a_i^{(n)} + \frac{k_r\Theta}{2\lambda}\right). \tag{A75b}$$

[1] J. C. Doyle and M. Csete, Architecture, constraints, and behavior, Proc. Natl. Acad. Sci. USA **108**, 15624 (2011).

[2] M. Kirschner and J. Gerhart, Evolvability, Proc. Natl. Acad. Sci. USA **95**, 8420 (1998).

[3] K. Joshi, C. S. Wright, K. F. Ziegler, E. M. Spiers, J. T. Crosser, S. Eschker, R. R. Biswas, and S. Iyer-Biswas, Emergent simplicities in stochastic intergenerational homeostasis, bioRxiv:10.1101/2023.01.18.524627.

[4] K. Joshi, R. R. Biswas, and S. Iyer-Biswas, Intergenerational scaling law determines the precision kinematics of stochastic individual-cell-size homeostasis, bioRxiv:10.1101/2023.01.20.525000.

[5] K. F. Ziegler, K. Joshi, C. S. Wright, S. Roy, W. Caruso, R. R. Biswas, and S. Iyer-Biswas, Scaling of stochastic growth and division dynamics: A comparative study of individual rod-shaped cells in the mother machine and schemostat platforms, Mol. Biol. Cell **35**, 1 (2024).

[6] C. S. Wright, K. Joshi, R. R. Biswas, and S. Iyer-Biswas, Emergent simplicities in the living histories of individual cells, arXiv:2404.01682 [Annu. Rev. Condens. Matter Phys. (to be published)].

[7] S. Iyer-Biswas, G. E. Crooks, N. F. Scherer, and A. R. Dinner, Universality in stochastic exponential growth, Phys. Rev. Lett. **113**, 028101 (2014).

[8] S. Iyer-Biswas, C. S. Wright, J. T. Henry, K. Lo, S. Burov, Y. Lin, G. E. Crooks, S. Crosson, A. R. Dinner, and N. F. Scherer, Scaling laws governing stochastic growth and division of single bacterial cells, Proc. Natl. Acad. Sci. USA **111**, 15912 (2014).

[9] C. N. Hinshelwood, On the chemical kinetics of autosynthetic systems, J. Chem. Soc. (Resumed) **11**, 745 (1952).

[10] D. Pirjol, F. Jafarpour, and S. Iyer-Biswas, Phenomenology of stochastic exponential growth, Phys. Rev. E **95**, 062406 (2017).

[11] N. Van Kampen, *Stochastic Processes in Physics and Chemistry*, 3rd ed. (Elsevier, Amsterdam, 2007).

[12] S. Iyer-Biswas, Applications of methods of non-equilibrium statistical physics to models of stochastic gene expression, Ph.D. thesis, Ohio State University, 2009.

[13] S. Iyer-Biswas, F. Hayot, and C. Jayaprakash, Stochasticity of gene products from transcriptional pulsing, Phys. Rev. E **79**, 031911 (2009).

[14] S. Iyer-Biswas and C. Jayaprakash, Mixed poisson distributions in exact solutions of stochastic autoregulation models, Phys. Rev. E **90**, 052712 (2014).

[15] J. Hu, S. Iyer-Biswas, S. C. Sealfon, J. Wetmur, C. Jayaprakash, and F. Hayot, Power-laws in interferon-B mRNA distribution in virus-infected dendritic cells, Biophys. J. **97**, 1984 (2009).

[16] S. Iyer-Biswas and A. Zilman, in *Advances in Chemical Physics*, edited by S. A. Rice and A. R. Dinner (Wiley, New York, 2016), Chap. 5, pp. 261–306.

[17] F. Jafarpour, M. Vennettilli, and S. Iyer-Biswas, Biological timekeeping in the presence of stochasticity, arXiv:1703.10058.

[18] S. Jun and S. Taheri-Araghi, Cell-size maintenance: Universal strategy revealed, Trends Microbiol. **23**, 4 (2015).

[19] A. Amir, Cell size regulation in bacteria, Phys. Rev. Lett. **112**, 208102 (2014).

[20] J. Lin and A. Amir, The effects of stochasticity at the single-cell level and cell size control on the population growth, Cell Syst. **5**, 358 (2017).

[21] T. W. Spiesser, C. Müller, G. Schreiber, M. Krantz, and E. Klipp, Size homeostasis can be intrinsic to growing cell populations and explained without size sensing or signalling, FEBS J. **279**, 4213 (2012).

[22] M. Deforet, D. van Ditmarsch, and J. B. Xavier, Cell-size homeostasis and the incremental rule in a bacterial pathogen, Biophys. J. **109**, 521 (2015).

[23] S. Taheri-Araghi, S. Bradde, J. T. Sauls, N. S. Hill, P. A. Levin, J. Paulsson, M. Vergassola, and S. Jun, Cell-size control and homeostasis in bacteria, Curr. Biol. **25**, 385 (2015).

[24] J. T. Sauls, D. Li, and S. Jun, Adder and a coarse-grained approach to cell size homeostasis in bacteria, Curr. Opin. Cell Biol. **38**, 38 (2016).

[25] M. M. Logsdon, P.-Y. Ho, K. Papavinasasundaram, K. Richardson, M. Cokol, C. M. Sassetti, A. Amir, and B. B. Aldridge, A parallel adder coordinates mycobacterial cell-cycle progression and cell-size homeostasis in the context of asymmetric growth and organization, Curr. Biol. **27**, 3367 (2017).

[26] L. Willis and K. C. Huang, Sizing up the bacterial cell cycle, Nat. Rev. Microbiol. **15**, 606 (2017).

[27] K. Joshi, K. F. Ziegler, S. Roy, C. S. Wright, R. Gandhi, J. Stonecipher, R. R. Biswas, and S. Iyer-Biswas, Non-Markovian memory and emergent simplicities in the stochastic and plastic adaptation of individual cells to dynamic environments, bioRxiv:10.1101/2023.05.27.542601.

[28] K. Joshi, S. Roy, R. R. Biswas, and S. Iyer-Biswas, Cellular dynamics under time-varying conditions, bioRxiv:10.1101/2023.03.07.531540.

[29] F. Jafarpour, C. S. Wright, H. Gudjonson, J. Riebling, E. Dawson, K. Lo, A. Fiebig, S. Crosson, A. R. Dinner, and S. Iyer-Biswas, Bridging the timescales of single-cell and population dynamics, Phys. Rev. X **8**, 021007 (2018).

[30] K. Joshi, H. York, C. S. Wright, R. R. Biswas, S. Arumugam, and S. Iyer-Biswas, Emergent spatiotemporal organization in stochastic intracellular transport dynamics, Ann. Rev. Biophys. **53**, 193 (2024).

[31] H. M. York, K. Joshi, C. S. Wright, L. Z. Kreplin, S. J. Rodgers, U. K. Moorthi, H. Gandhi, A. Patil, C. A. Mitchell, S. Iyer-Biswas, and S. Arumugam, Deterministic early endosomal maturations emerge from a stochastic trigger-and-convert mechanism, Nat. Commun. **14**, 4652 (2023).

[32] S. Sanders, K. Joshi, P. A. Levin, and S. Iyer-Biswas, Beyond the average: An updated framework for understanding the relationship between cell growth, DNA replication, and division in a bacterial system, PLoS Genet. **19**, e1010505 (2023).

[33] D. P. Haeusser and W. Margolin, Splitsville: Structural and functional insights into the dynamic bacterial Z ring, Nat. Rev. Microbiol. **14**, 305 (2016).

[34] R. M. Teather, J. F. Collins, and W. D. Donachie, Quantal behavior of a diffusible factor which initiates septum formation at potential division sites in *Escherichia coli*, J. Bacteriol. **118**, 407 (1974).

[35] A.-C. Chien, N. S. Hill, and P. A. Levin, Cell size control in bacteria, Curr. Biol. **22**, R340 (2012).

[36] M. Aaron, G. Charbon, H. Lam, H. Schwarz, W. Vollmer, and C. Jacobs-Wagner, The tubulin homologue FtsZ contributes to cell elongation by guiding cell wall precursor synthesis in *Caulobacter crescentus*, Mol. Microbiol. **64**, 938 (2007).

[37] E. D. Goley, Y.-C. Yeh, S.-H. Hong, M. J. Fero, E. Abeliuk, H. H. McAdams, and L. Shapiro, Assembly of the *Caulobacter* cell division machine, Mol. Microbiol. **80**, 1680 (2011).

[38] D. W. Adams and J. Errington, Bacterial cell division: Assembly, maintenance and disassembly of the Z ring, Nat. Rev. Microbiol. **7**, 642 (2009).

[39] J. M. Wagstaff, M. Tsim, M. A. Oliva, A. García-Sanchez, D. Kureisaite-Ciziene, J. M. Andreu, and J. Löwe, A polymerization-associated structural switch in FtsZ that enables treadmilling of model filaments, mBio **8**, 16 (2017).

[40] Y. Chen and H. P. Erickson, Rapid *in vitro* assembly dynamics and subunit turnover of FtsZ demonstrated by fluorescence resonance energy transfer, J. Biol. Chem. **280**, 22549 (2005).

[41] G. Lan, A. Dajkovic, D. Wirtz, and S. X. Sun, Polymerization and bundling kinetics of FtsZ filaments, Biophys. J. **95**, 4045 (2008).

[42] M. Loose and T. J. Mitchison, The bacterial cell division proteins FtsA and FtsZ self-organize into dynamic cytoskeletal patterns, Nat. Cell Biol. **16**, 38 (2014).

[43] J. M. Barrows and E. D. Goley, FtsZ dynamics in bacterial division: What, how, and why? Curr. Opin. Cell Biol. **68**, 163 (2021).

[44] X. Yang, Z. Lyu, A. Miguel, R. McQuillen, K. C. Huang, and J. Xiao, GTPase activity–coupled treadmilling of the bacterial tubulin FtsZ organizes septal cell wall synthesis, Science **355**, 744 (2017).

[45] A. W. Bisson-Filho, Y.-P. Hsu, G. R. Squyres, E. Kuru, F. Wu, C. Jukes, Y. Sun, C. Dekker, S. Holden, M. S. VanNieuwenhze, Y. V. Brun, and E. C. Garner, Treadmilling by FtsZ filaments drives peptidoglycan synthesis and bacterial cell division, Science **355**, 739 (2017).

[46] P. J. Lariviere, C. R. Mahone, G. Santiago-Collazo, M. Howell, A. K. Daitch, R. Zeinert, P. Chien, P. J. B. Brown, and E. D. Goley, An essential regulator of bacterial division links FtsZ to cell wall synthase activation, Curr. Biol. **29**, 1460 (2019).

[47] K. D. Whitley, C. Jukes, N. Tregidgo, E. Karinou, P. Almada, Y. Cesbron, R. Henriques, C. Dekker, and S. Holden, FtsZ treadmilling is essential for Z-ring condensation and septal constriction initiation in *Bacillus subtilis* cell division, Nat. Commun. **12**, 2448 (2021).

[48] R. McQuillen and J. Xiao, Insights into the structure, function, and dynamics of the bacterial cytokinetic FtsZ-ring, Annu. Rev. Biophys. **49**, 309 (2020).

[49] S. G. Addinall and B. Holland, The tubulin ancestor, FtsZ, draughtsman, designer and driving force for bacterial cytokinesis, J. Mol. Biol. **318**, 219 (2002).

[50] F. Si, G. Le Treut, J. T. Sauls, S. Vadia, P. A. Levin, and S. Jun, Mechanistic origin of cell-size control and homeostasis in bacteria, Curr. Biol. **29**, 1760 (2019).

[51] J. Männik, B. E. Walker, and J. Männik, Cell cycle-dependent regulation of FtsZ in *Escherichia coli* in slow growth conditions, Mol. Microbiol. **110**, 1030 (2018).

[52] S. K. Govers, M. Campos, B. Tyagi, G. Laloux, and C. Jacobs-Wagner, Apparent simplicity and emergent robustness in bacterial cell cycle control, Cell Syst. **15**, 19 (2023).

[53] M. T. Laub, H. H. McAdams, T. Feldblyum, C. M. Fraser, and L. Shapiro, Global analysis of the genetic network controlling a bacterial cell cycle, Science **290**, 2144 (2000).

[54] E. Quardokus, N. Din, and Y. V. Brun, Cell cycle regulation and cell type-specific localization of the FtsZ division initiation protein in *Caulobacter*, Proc. Natl. Acad. Sci. USA **93**, 6314 (1996).

[55] A. J. Kelly, M. J. Sackett, N. Din, E. Quardokus, and Y. V. Brun, Cell cycle-dependent transcriptional and proteolytic regulation of FtsZ in *Caulobacter*, Genes Dev. **12**, 880 (1998).

[56] J. Collier, Cell division control in *Caulobacter crescentus*, Biochim. Biophys. Acta Gene Regul. Mech. **1862**, 685 (2019).

[57] M. E. Martin, M. J. Trimble, and Y. V. Brun, Cell cycle-dependent abundance, stability and localization of FtsA and FtsQ in *Caulobacter crescentus*, Mol. Microbiol. **54**, 60 (2004).

[58] B. Williams, N. Bhat, P. Chien, and L. Shapiro, ClpXP and ClpAP proteolytic activity on divisome substrates is differentially regulated following the *Caulobacter* asymmetric cell division, Mol. Microbiol. **93**, 853 (2014).

[59] S. Garde, P. K. Chodisetti, and M. Reddy, Peptidoglycan: Structure, synthesis, and regulation, EcoSal Plus **9**, 35 (2021).

[60] L. K. Harris and J. A. Theriot, Relative rates of surface and volume synthesis set bacterial cell size, Cell **165**, 1479 (2016).

[61] A. Typas, M. Banzhaf, C. A. Gross, and W. Vollmer, From the regulation of peptidoglycan synthesis to bacterial growth and morphology, Nat. Rev. Microbiol. **10**, 123 (2012).

[62] M. C. F. van Teeseling, Elongation at midcell in preparation of cell division requires FtsZ, but not MreB nor PBP2 in *Caulobacter crescentus*, Front. Microbiol. **12**, 732031 (2021).

[63] M. A. de Pedro, J. C. Quintela, J. V. Höltje, and H. Schwarz, Murein segregation in Escherichia coli, J. Bacteriol. **179**, 2823 (1997).

[64] P. P. Navarro, A. Vettiger, V. Y. Ananda, P. M. Llopis, C. Allolio, T. G. Bernhardt, and L. H. Chao, Cell wall synthesis and remodelling dynamics determine division site architecture and cell shape in *Escherichia coli*, Nat. Microbiol. **7**, 1621 (2022).

[65] N. Baranova, P. Radler, V. M. Hernández-Rocamora, C. Alfonso, M. López-Pelegrín, G. Rivas, W. Vollmer, and M. Loose, Diffusion and capture permits dynamic coupling between treadmilling FtsZ filaments and cell division proteins, Nat. Microbiol. **5**, 407 (2020).

[66] E. Schrödinger, Zur theorie der fall- und steigversuche an teilchen mit Brownscher bewegung, Phys. Z. **16**, 289 (1915).

[67] A. Lambert, A. Vanhecke, A. Archetti, S. Holden, F. Schaber, Z. Pincus, M. T. Laub, E. Goley, and S. Manley, Constriction rate modulation can drive cell size control and homeostasis in *C. crescentus*, iScience **4**, 180 (2018).

[68] C. Jia, A. Singh, and R. Grima, Cell size distribution of lineage data: Analytic results and parameter inference, iScience **24**, 102220 (2021).

[69] C. Jia, A. Singh, and R. Grima, Characterizing non-exponential growth and bimodal cell size distributions in fission yeast: An analytical approach, PLoS Comput. Biol. **18**, e1009793 (2022).